HIGH SPEED ATOMIC FORCE MICROSCOPY (HS-AFM): DIRECT VISUALIZATION OF THE OUTER MEMBRANE PHOSPHOLIPASE A (OMPLA) ACTIVITY

LUCA RIMA

Thesis for the Master of Science in Nanosciences

Experiments have been carried out in the Bio-AFM-Lab (U1006 INSERM) at the Aix-Marseille University

March – August 2016

Luca Rima: *High Speed Atomic Force Microscopy (HS-AFM): Direct Visualization of the Outer Membrane Phospholipase A (OmpLA) Activity,* Thesis for the Master of Science in Nanosciences, Marseille, March – August 2016 ©

SUPERVISORS:
Prof. Dr. Henning Stahlberg
Prof. Dr. Simon Scheuring
Dr. Martina Rangl

ABSTRACT

Phospholipases play a key role in various physiological processes such as proliferation, digestion or neural activation. These enzymes are widely expressed within different cell types and cell locations and show diverse working mechanisms and different functions. The outer membrane phospholipase A (OmpLA) is one of the rare enzymes located in the outer membrane of Gram-negative bacteria and is associated with membrane transport and bacterial virulence. It is regulated by calcium and it forms dimers in the active state. Despite knowing the structure of OmpLA since the late 90s, its biological function and its role in different physiological transactions is still not fully understood. To elucidate the working mechanism of this bacterial lipase we used high-speed atomic force microscopy (HS-AFM) to monitor OmpLA during function. HS-AFM has evolved in a powerful tool for studying single molecules at work under physiological conditions with high lateral (nm) and temporal resolution (ms). In this study we report the direct visualization of OmpLA-induced and Ca^2-dependent shrinking of lipid patches in real time.

ACKNOWLEDGEMENTS

I want to thank all who made this project possible:
Prof. Dr. Simon Scheuring for giving me the opportunity to work in his laboratory.
Prof. Dr. Henning Stahlberg for his supervision at the University of Basel.
Dr. Martina Rangl for her great support during the whole project.
The Swiss Nanoscience Institute for supporting my master's thesis.
Dr. Katrein Spieler, Jacqueline Isenburg, Sophie Gall and Véronique Preau for helping me organizing the project.
I also want to express my gratitude to all members of the Bio-AFM-Lab U1006 for the pleasant work evironment during the last months.

CONTENTS

1 INTRODUCTION 1

2 THEORY 3

2.1 High-Speed Atomic Force Microscopy (HS-AFM) . . . 3

2.1.1 Atomic Force Microscopy (AFM) 3

2.1.2 Development of HS-AFM 5

2.1.3 HS-AFM Setup 7

2.1.4 Imaging Speed of Bio-HS-AFM 9

2.2 Outer Membrane Phospholipase A (OmpLA) 10

2.2.1 Structure 11

2.2.2 Function 12

3 MATERIALS AND METHODS 15

3.1 Materials 15

3.1.1 HS-AFM 1.0 - Ando Model 15

3.1.2 Cantilevers, Chemicals 16

3.1.3 Additional Devices 18

3.2 Data Analysis 18

3.3 Experimental Methods 18

3.3.1 HS-AFM Imaging 18

3.3.2 Sample Preparation 19

3.3.3 Pumping System 20

3.3.4 Tip Cleaning 20

4 RESULTS AND DISCUSSION 23

4.1 Membrane Degradation 23

4.2 Membrane Degradation is Protein-induced 28

4.3 Membrane Degradation is Calcium-dependent 28

4.4 OmpLA alignment Lipid-dependent 29

4.5 OmpLA Integration into DLPC 31

5 CONCLUSION 35

BIBLIOGRAPHY 37

A APPENDIX 45

A.1 Opening of Liposomes 45

A.2 Change in Appearance of OmpLA is reversible 46

NOMENCLATURE

AFM Atomic-force microscopy

DLPC 1,2-dilauroyl-sn-glycero-3-phosphocholine

DNA Deoxyribonucleic acid

EDTA Ethylenediaminetetraacetic acid

F_6OPC 3,3,4,4,5,5,6,6,7,7,8,8,8-tridecafluoro-*n*-octylphosphocholine

fps Frames per second

IMP Integral membrane protein

LD Laser diode

LP Lipoprotein

LPS Lipopolysaccharide

OBD Optical beam deflection

OMP Outer membrane protein

OmpLA Outer membrane phopholipase A

PCI Peripheral Component Interconnect

PID Proportional–integral–derivative

POPC 1-palmitoyl-2-oleoyl-sn-glycero-3-phosphocholine

Q-controller Quality factor controller

STM Scanning tunneling microscope

Tris Tris(hydroxymethyl)aminomethane

LIST OF FIGURES

Figure 1 Gram-negative cell wall structure 1
Figure 2 AFM setup 4
Figure 3 Amplitude and phase response curve 5
Figure 4 Speed comparison 6
Figure 5 HS-AFM schematic 7
Figure 6 HS-AFM scanner 9
Figure 7 Feedback delay consequences 10
Figure 8 OmpLA structure 12
Figure 9 Working principle OmpLA. 13
Figure 10 HS-AFM setup 16
Figure 11 Scanner and cantilever holder 16
Figure 12 Cantilever and tip 17
Figure 13 Glass rod preparation 19
Figure 14 Sample incubation 20
Figure 15 Pumping system 20
Figure 16 Plasma cleaner 21
Figure 17 Ca^{2+} induced OmpLA activation. 24
Figure 18 OmpLA in presence EDTA. 25
Figure 19 OmpLA in presence of Ca^{2+} 25
Figure 20 Membrane degradation 26
Figure 21 Pumping system experiment 26
Figure 22 Graph pumping system 27
Figure 23 Overview tubular structures 27
Figure 24 Control experiment without protein 28
Figure 25 Control experiment with magnesium 29
Figure 26 Crystal 30
Figure 27 Crystal 31
Figure 28 Densely packed OmpLA membrane 31
Figure 29 OmpLA integration 1 32
Figure 30 OmpLA integration 2 32
Figure 31 OmpLA integration close-up view 33
Figure 32 Opening DLPC proteoliposome 45
Figure 33 Reversible appearance 46

1 INTRODUCTION

Biological membranes play a key role in cells and therefore also for life in general. They are basically composed of phospholipids, proteins and some other lipid molecules like glycolipids or cholesterol. Biological membranes are responsible for the formation and separation of biological compartments, maintaining electrochemical gradients, secretion and uptake of nutrients and metabolites, control of enzymatic activities, signal transduction and control of cell mobility and adhesion [38]. In most of these processes membrane proteins are directly involved. The high importance of those membrane proteins is reflected by the fact that ~30% of the proteome is made up by membrane proteins [22]. Therefore, the investigation of membrane proteins is crucial to gain new insights into many biological processes. However, only ~3% [55] of the determined structures in the protein data bank are membrane proteins due to the difficulties in membrane protein expression, sample preparation and investigation.

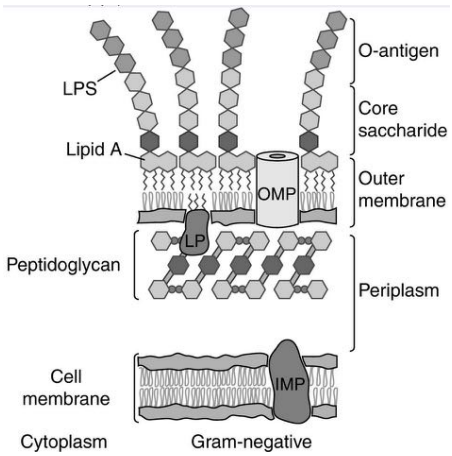

Figure 1: Cell wall structure of Gram-negative bacteria. IMP = integral membrane protein; LP = lipoprotein; LPS = lipopolysaccharide; OMP = outer membrane protein. Figure taken from Silhavy et al. [61].

For determining the structures of proteins the prevalent experimental methods are X-Ray crystallography, nuclear magnetic resonance (NMR) spectroscopy and electron microscopy in descending order. Electron microscopy recently attracted huge attention due to the development of new direct electron detectors which significantly improved the capabilities of this technique. A drawback of all these methods, however, is the lack of possibility to image and study proteins in their native environment with a high temporal resolution. In contrast fluorescent microscopy allows investigating proteins in liq-

uid, and thus in an active state. The resolution of this technique, however, is not as good as the resolution of the methods mentioned before and the protein of interest has to be fluorescently labeled. Hence, it is not possible to directly visualize proteins in action. Fortunately, this gap can now be filled by the application of high speed atomic force microscopy (HS-AFM). This technique allows imaging proteins in a native-like environment at a spatial and temporal resolution of about 1 nm and 100 ms enabling to monitor single molecules at video frame rate. Accordingly, it is possible for the first time to observe the dynamics of single proteins at work. These properties made HS-AFM an attractive tool to study the outer membrane phopholipase A (OmpLA). The main function of OmpLA is the detection of defects caused by phospholipids in the outer leaflet of the outer membrane in Gram-negative bacteria and the subsequent hydrolysis of those phospholipids (see Figure 1). The structure of OmpLA was determined by X-ray crystallography in 1999 [63] but the biological function is still not fully understood. Therefore, HS-AFM was used to gain new insights into the working principle of OmpLA. In this study, we demonstrated for the first time the OmpLA induced shrinking of lipid bilayers.

2 THEORY

2.1 HIGH-SPEED ATOMIC FORCE MICROSCOPY (HS-AFM)

The following sections describe the principles of atomic force microscopy (AFM). In the first section the history and working principle of AFM are described. The second section is about the development of high-speed AFM. In the third section the HS-AFM setup, the cantilevers and the HS-scanner are explained in more detail. Finally, the last section gives some information about the speed limitations for high speed imaging of biological samples.

2.1.1 *Atomic Force Microscopy (AFM)*

Atomic force microscopy is a form of scanning probe microscopy (SPM). The development of SPM began in the 80s by the invention of the scanning tunneling microscope (STM) which exploits tunneling currents for the formation of an image [9]. Three years after that, a second form of SPM, the AFM, was developed [8]. As implied by the name, the AFM is using forces between a sharp tip and a sample to generate an image. In contrast to STM an AFM is capable of imaging non-conductive surfaces, and thus increasing the number of potential samples. Beside imaging, AFM is also capable of manipulating samples and measuring forces (*aka* force spectroscopy). For imaging several different modes were developed and are classified into contact mode, intermittent contact mode and noncontact mode. For biological samples the intermittent contact mode is the most prevalent one. A schematic of an intermittent contact mode HS-AFM setup is depicted in Figure 2. This mode was also used during this project. Therefore, it is described in more detail in the following part.

In intermittent contact mode (also tapping or amplitude modulation (AM) mode) [74], the cantilever is excited at a constant frequency near its resonance frequency. When the tip is interacting with the sample the amplitude is decreased due to energy dissipation and altered due to a resonance frequency shift of the cantilever in the following way. If f_c is the original resonance frequency, k_c the spring constant and k the gradient of the tip-sample interaction force in Z-direction then the shift (Δf_c) of the resonance frequency can be approximated by [4]

$$\Delta f_c = -(f_c/2k_c)k \tag{1}$$

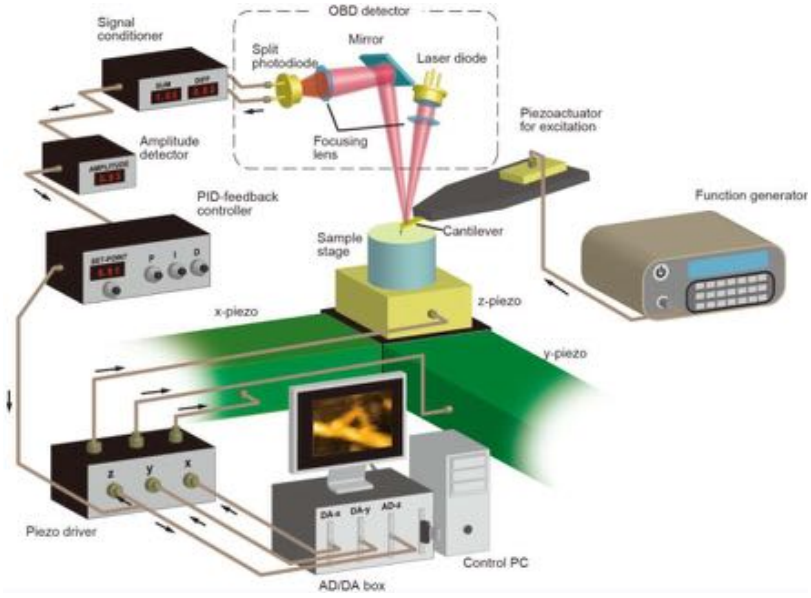

Figure 2: Schematic of an intermittent contact mode HS-AFM setup. Figure taken from Ando et al. 2014 [4]

This equation shows, that the resonant frequency of the cantilever is increased by repulsive tip-sample interactions and that the magnitude of the shift depends on the f_c/k_c ratio. This is significant for HS-AFM due to the high resonant frequencies and small spring constants of small cantilevers. This shift of the resonant frequency leads to an increase or decrease of the oscillation amplitude depending on the excitation frequency f_{ex} and a phase shift relative to the excitation signal (see Figure 3).

A feedback control is used for maintaining a constant set point amplitude (A_s) while scanning. For biological samples A_s should be above 80% of the free oscillation amplitude (A_0) to ensure non-invasive scanning. The set point force F_s can be approximated by [56]

$$F_s = k_c[(1-\alpha) \times (A_0^2 - A_s^2)]^{1/2}/Q_c \tag{2}$$

where Q_c is the quality factor and α ($0 < \alpha < 1$) the ratio of amplitude reduction from the resonance frequency shift over the total reduction of the amplitude (For HS-AFM $\alpha =\sim 0.5$ [4]). As described in Section 2.1.4, F_s is varying while scanning depending on if it is an uphill or downhill area of the sample. It is noteworthy, that the set point force F_s is not the most important quantity influencing the sample, but the impulsive force. The impulsive force is the integral of the force over the time interval during which it acts, in other words, the time the tip is interacting with the sample which is only about 10% of the time of an oscillation cycle. Because small cantilevers used for HS-AFM have high resonant frequencies, this time interval is very short resulting in very small impulsive forces in the atto-Newton sec-

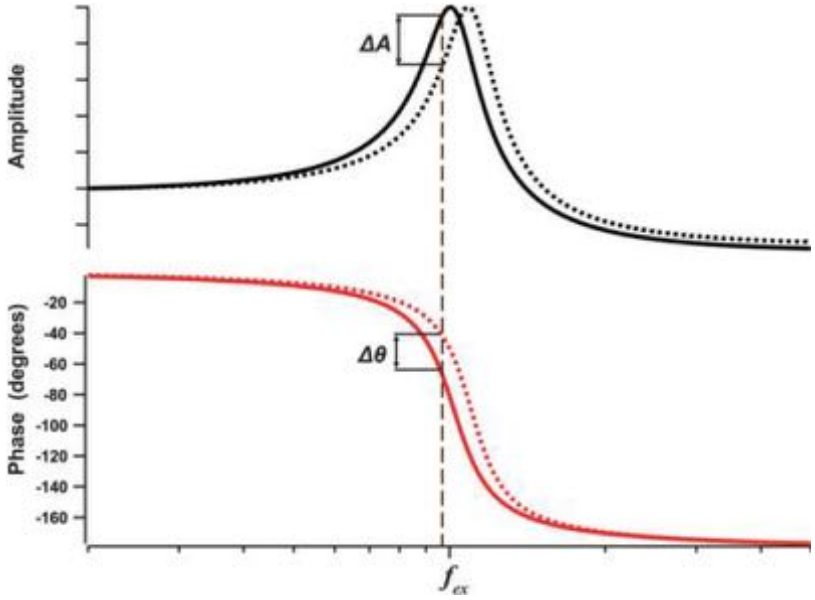

Figure 3: Cantilever response to a shift in the resonance frequency. Solid line: Free oscillation; Broken line: Influence of a negative force gradient (no energy dissipation). Δf_c is resulting in a shift of the amplitude and a phase shift relative to the excitation. In this figure, a repulsive tip-sample interaction is leading to an increase of the cantilever resonance frequency and therefore to a decrease of the amplitude by ΔA and a phase advance of $\Delta\Theta$ when the cantilever is excited at f_{ex}. Figure taken from Ando et al. 2014 [4].

ond range [4]. The deflection of the cantilever is measured using an optical beam deflection (OBD) system that detects the position of a laserspot on a photodiode sensor which was previously reflected on the back of the cantilever. After a deflection-to-amplitude converter, the amplitude is subtracted from the set point amplitude. The difference is the feedback error. The proportional-integral-derivative (PID) then drives the Z-piezodriver to eliminate the feedback error by displacing the Z-piezo. The output of the PID controller corresponds to the sample height. Combining this information with the X- and Y-position of the tip an image can be generated.

2.1.2 *Development of HS-AFM*

Conventional atomic force microscopy (AFM) was already capable of imaging biological samples in physiological conditions. The problem was that biological processes often occur at milliseconds to seconds time-scale which is too fast for a conventional AFM which needs minutes to create an image (see Figure 4). Therefore, many attempts have been made to increase the imaging speed of AFM and thereby preserving the advantages (*e.g.* direct imaging of the sample, high spatial resolution, measuring in physiological conditions) of this technique [36].

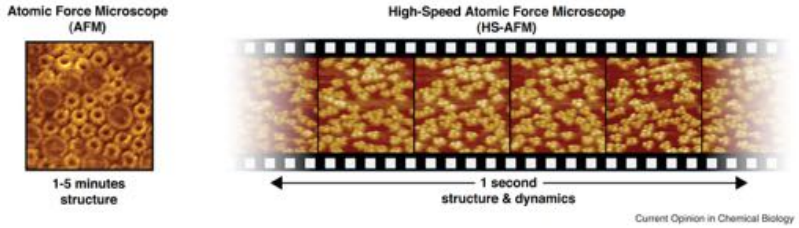

Figure 4: Comparison of the imaging rates achieved by HS-AFM and conventional AFM. Figure taken from Casuso et al. 2011 [12].

The beginning of the development of fast scanning AFM was in the early 90s [7] and focused on the investigation and lithography of hard surfaces. Later on, cantilevers with integrated actuators and sensors were used in order to increase the imaging speed [45, 64]. The best mode for imaging biological samples is the tapping mode. The main speed limitations of this mode are the reaction speed and resonance frequency of the cantilever. This problem was addressed through the integration of faster feedback actuators and the active control of the dynamics of the cantilever [65]. During the last 20 years three groups contributed a lot to the development of HS-AFM: The Ando group, the Miles group and the Hansma group. They refined a lot of the techniques and presented new approaches. In 1996 the Hansma group presented short cantilevers for high speed imaging [71] and a suitable optical deflection detector [59]. Three years later, they imaged DNA in 1.7 seconds per frame [69] and in 2000 the dissociation of GroES-GroEL complexes [70]. Ando and co-workers presented their HS-AFM in 2001 [1] together with small cantilevers and a suitable OBD. Their system comprised a high speed scanner, fast electronics and a dynamic feedback loop. More information about this HS-AFM setup are given in Section 2.1.3. Further along the line the Hansma group also demonstrated high speed scanners and fast data acquisition systems [23, 24, 39]. The group of Miles was using a tuning fork as X-Scanner in 2005 [35], developed a fast digital processing system to obtain cantilever deflection data and achieved imaging rates of 1300 frames per second in constant-height mode of fixed collagen fibers [53]. The development of HS-AFM is still an ongoing process. The HS-AFM 1.0 - Ando model is now commercially available but still attempts are made to further improve HS-AFM systems. The Scheuring group recently optimized the HS-setup for biological applications by implementing a buffer exchanging system [49], a temperature control add-on allowing to study the phase transition of lipids and an automated force controller keeping the applied force constantly and automatically constant with pico Newton precision [48]. Another approach is to combine HS-AFM with other microscopy techniques like optical- and fluorescence microscopy to increase the range of applications. Many biological phenomena were studied for the first time in

the recent past like walking Myosin V [43], diffusion of OmpF [13], the deformation of membranes by ESCRT-III [15], the spatiotemporal dynamic of the nuclear pore complex transport barrier [57] and many more.

2.1.3 *HS-AFM Setup*

The working principle of an HS-AFM is roughly the same as for a conventional AFM but several parts have to be modified in order to meet the requirements of high speed imaging (see Figure 5). The most important changes were the development of small cantilevers, a fast scanner and a dynamic PID control. The cantilevers and the scanner are described in more detail in the following parts.

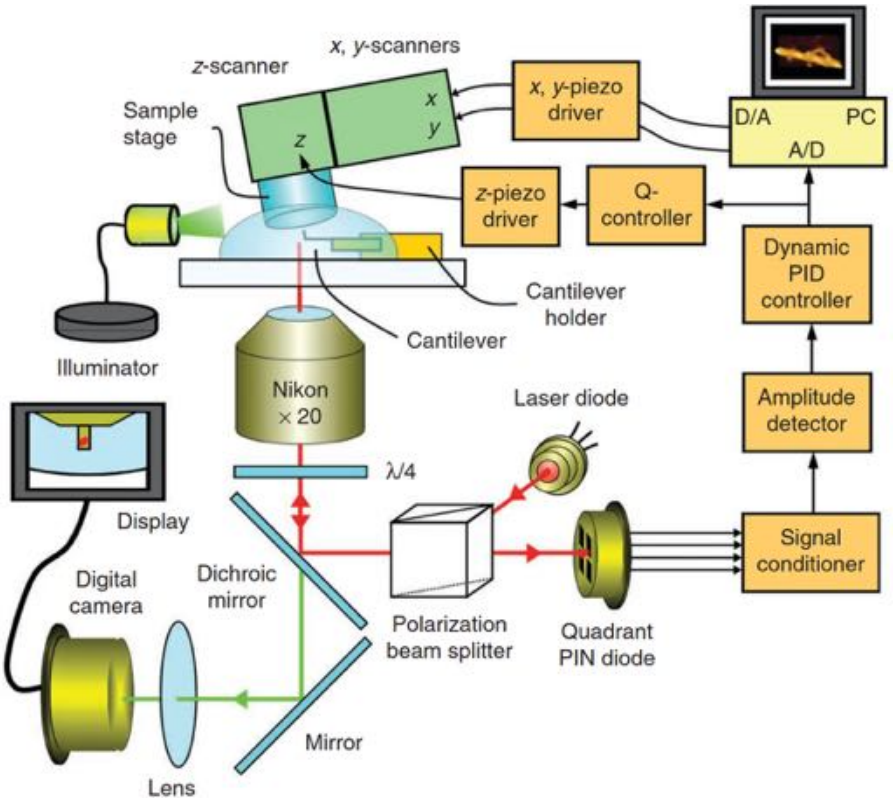

Figure 5: HS-AFM system. Figure taken from Uchihashi et al. 2012 [68].

2.1.3.1 *Cantilevers*

One of the most important steps in the development of HS-AFM was the production of small cantilevers. High speed scanning requires a fast response speed of the cantilever. Therefore, small cantilevers are favourable because the response speed scales with the inverse of the square root of the mass ($\sim 1/\sqrt{m}$) [36]. Also, a high resonance

frequency (f_c) and a low spring constant (k_c) are a necessity for biological HS-AFM applications. They can be calculated by

$$f_c = 0.56\frac{d}{L^2}\sqrt{\frac{E}{12\rho}} \tag{3}$$

$$k_c = \frac{wd^3}{4L^3}E \tag{4}$$

Where ρ is the density and E the Young's modulus of the cantilever material, d the thickness, w the width and L the length of the cantilever. As mentioned before (see Section 2.1.1) the high resonance frequency and low spring constant also leading to a huge f_c/k_c ratio providing high sensitivity for tip-sample interaction detection. Another benefit of small cantilevers is that the amplitude detection is hardly affected by thermal noise effects. According to the equipartition theorem, thermal excitation deflects the cantilever at the free end (Δz) by [4]

$$< z^2 >^{1/2} = (k_B T/k_c)^{1/2} \tag{5}$$

The averaged thermal deflection values are similar to the amplitude damping (A_0-A_s) but the thermal noise is distributed over a huge frequency range of $\sim 0 - 2f_c$ and therefore the thermal noise density is small. Also a bandpass filter can eliminate most of the thermal noise by filtering the differential output signal of the photodiode because the frequency region used for imaging lies only around f_c. Another advantage of small cantilevers or in this case short cantilevers is the increased change of the angle ($\Delta\varphi$) upon deflection [4]

$$\Delta\varphi = 3\Delta z/2L \tag{6}$$

Where Δz is displacement of the cantilever free end in Z-direction and L the length of the cantilever. This improves the detection sensitivity of the OBD system and allows better force control.

2.1.3.2 *Scanner*

For HS-AFM new scanners were developed. These scanners are optimized for fast scanning without causing disturbances. This is achieved by a sophisticated design of the scanner (see Figure 6). Flexure stages made of blade springs for the x and y scanner were manufactured by monolithic processing in order to minimize the number of resonant peaks [5, 6]. The x-scanner is displaced by the y-scanner and the z-scanner is displaced by the x-scanner. On top of the z-scanner a sample stage (glass rod) is mounted. The x-piezo is placed in between two flexures in order to fix the center of mass and therefore suppress mechanical excitation [6]. Besides the z-piezo and the sample stage,

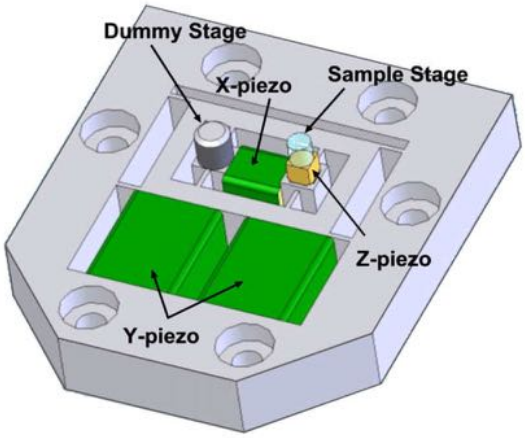

Figure 6: HS-AFM scanner. Figure taken from Ando et al. 2008 [2].

the x-piezo also displaces a dummy stage acting as a counterbalance. The z-piezo is held at the corners perpendicular to the displacement direction. Therefore, it can be displaced in both directions. This is desirable, because like this the resonant frequency of the piezo is not lowered but the displacement is reduced by half. Another advantage of this mounting is that impulsive forces are hardly exerted on the scanner, therefore, nearly no mechanical excitation is produced [6]. Active damping is also incorporated in the scanner: For the x-scanner either by Q-control technique [42] or by feedforward control using inverse compensation [60, 75] and for the z-scanner by Q-control technique or by inverse compensation.

2.1.4 *Imaging Speed of Bio-HS-AFM*

The feedback control has an inherent time delay (τ_0). This is affecting the imaging speed in the following way [3]. To describe the problem, the surface of the sample is assumed to be sinusoidal with a periodicity of λ. The scan velocity is V_s. Therefore, the height of the sample changes at a frequency of $f = Vs/\lambda$. The phase delay of the Z-scanner is $\Theta = 2\Pi f\tau_0$ (see Figure 7a). Because of this delay, in the uphill region of the sample the amplitude (A) is smaller than the setpoint amplitude (A_s) whereas in the the downhill region the amplitude is bigger than the setpoint amplitude. Regarding Equation 2, this means that the force is higher in the uphill region than in the downhill region (see Figure 7b). For biological samples the force should not be too high, but by lowering the setpoint force for minimizing the force in the uphill regions too much, the force in the downhill region may become zero (see Figure 7c) because the tip loses contact with the surface and the amplitude equals the free oscillation amplitude. Therefore the error signal is saturated at a small value and it takes a long time to bring the tip back in contact. This effect is also called parachut-

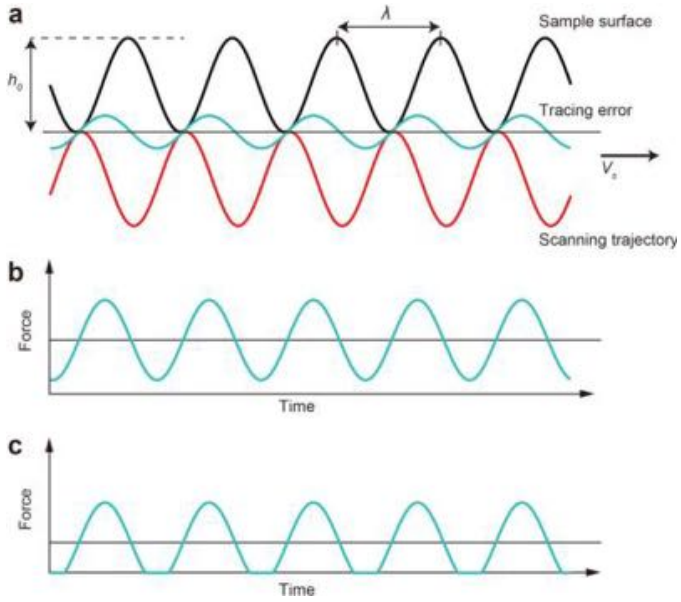

Figure 7: Tip-sample forces due to the feedback delay. a) Black line: Sample surface; Red Line: Z-scanner movement; Blue line: Tracing Error. b) Blue line: Tip-sample force; Black line: Large set point force. c) Blue line: Tip-sample force; Black line: Small set point force. Note that the force equals 0 in the downhill regions of the sample. Figure taken from Ando et al. 2014 [4].

ing. So the phase delay is responsible for excessive force in the uphill region and for parachuting in the downhill regions but the acceptable phase delay for avoiding parachuting is ~10 times lower than for producing too much force [3, 4, 68]. Thus parachuting is the bottleneck for high speed imaging of biological samples. This problem has been solved by the development of a dynamic PID control which adds a false error signal to the real error signal when the amplitude is bigger than the setpoint amplitude [41]. Because the feedback phase delay is the crucial parameter for imaging biological samples it follows that the highest possible feedback frequency is $f_{max} = \Theta_{max}/(2\Pi\tau_0)$ (Θ_{max} is the maximum allowable phase delay), the highest possible scan velocity is $V_s^{max} = \lambda\Theta_{max}/(2\Pi\tau_0)$ and if W is the width of the picture and N the number of scan lines the highest possible imaging rate is [4]

$$R_{max} = \lambda\Theta_{max}/(4\pi NW\tau_0) \tag{7}$$

2.2 OUTER MEMBRANE PHOSPHOLIPASE A (OMPLA)

Outer membrane phospholipase A (OmpLA) is one of the rare enzymes located in the outer membrane of Gram-negative bacteria. It was first purified in 1971 [58]. The phospholipase shows A_1, A_2, L_1 and L_2 activity [33, 50, 58]. OmpLA forms dimers upon activation triggered by the presence of phopholipids and calcium in the outer leaflet of the outer membrane which normally only contains

lipopolysaccharides (LPS). In the following two sections, the structure and the function of OmpLA are described in more detail.

2.2.1 *Structure*

Monomeric OmpLA has a β-barrel consisting of 12 antiparallel strands with a flat and a convex side. The dimensions are $\sim 20 \times 30 \times 45$ Å^3 (see Figure 8). The β-barrel has hydrophobic surface for the integration in the membrane and exhibit two regions with aromatic residues at the polar-apolar boundaries of the membrane bilayer (aromatic girdle). Inside the β-barrel an intricate hydrogen-bonding network provides a rigid structure [63]. The cavity is occluded [10]. The termini and turns are located at the periplasmic side while the loop region is at the extracellular side [47]. The active site residues Asn156, His142 and Ser144 [11, 32, 40] are located on the exterior of the β-barrel just outside the outer leaflet ring of aromatic residues [63] (see Figure 8A). Therefore, normally no substrate is in the vicinity of the active site because phospholipids are only present in the inner leaflet of the outer membrane. The active site resembles a classical serine hydrolase [21] but the aspartate is substituted with an asparagine in *E. coli*. In the monomeric state OmpLA is inactive. The dimer is the active form [19]. This regulatory dimerization mechanism is described in more detail in Section 2.2.2. OmpLA is forming homodimers by the association of two monomers at their flat barrel side (see Figure 8C,D) [63]. The structure of OmpLA in the dimeric state shows nearly no difference to the monomeric state. By forming the dimer, two substrate binding pockets are formed, allowing OmpLA to bind one acyl chain of a variety of different substrates with one or two acyl chains. These binding pockets are the reason that OmpLA is only active as a dimer [63].

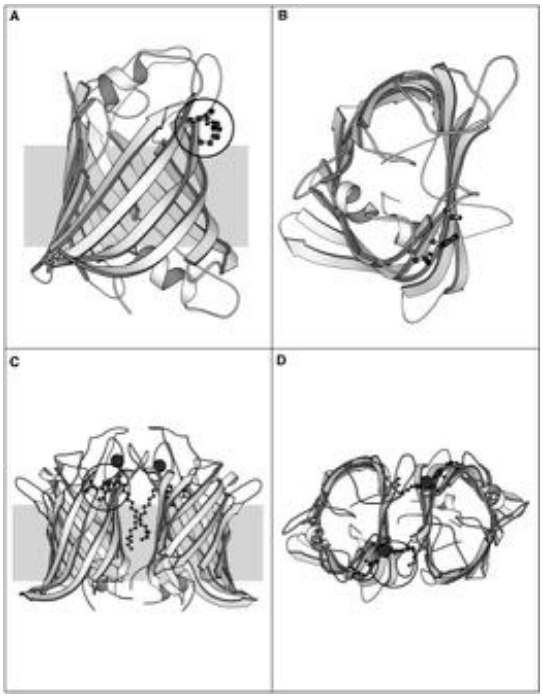

Figure 8: X-ray crystallographic structure of OmpLA (Snijder et al. [63]). A) Side view of monomeric OmpLA (pdb code 1qd5). The active site is indicated by a circle. B) Top view of monomeric OmpLA. C) Side view of dimeric OmpLA (pdb code 1qd6). Ca^{2+} is shown as black spheres, the inhibitor hexadecanesulphonyl fluoride is shown as ball-and-stick model. D) Top view of dimeric OmpLA. One of the two active sites is indicated by a circle. Figure taken from Dekker 2000 [18].

2.2.2 *Function*

In an intact outer mebrane, OmpLA is in its inactive monomeric state. If the cofactor Ca^{2+} [19] and substrate [67] is available at the same time, it forms enzymatic active homodimers. As usually *in vivo* Ca^{2+} is available most of the time it is likely that the substrate controls dimerization, and thus the activity. Because in the experiments of this project phospholipids were present all the time, EDTA was used to bind residual Ca^{2+} to keep OmpLA in its monomeric inactive state and trigger the activity of OmpLA by the addition of Ca^{2+}. *In vivo* however, perturbations of the outer membrane are responsible for the activation of OmpLA because they are leading to the presence of phospholipids in the outer leaflet of the outer membrane. Potential origins of perturbations are heat shock [28], spheroplast formation [51], phage-induced lysis [16], transfection of phage DNA [66], EDTA-treatment [29] and the action of antimicrobial peptides/proteins [72, 73]. The presentation of substrate to the active site of OmpLA triggers the dimerisation and an active dimer-substrate-cofactor complex is created. In this complex a nucleophilic attack of Ser144 on the carbonyl carbon of the ester is performed. Ca^{2+} supports this by the polarisation of the ester carbonyl bond. The resulting intermediate is stabilized by Ca^{2+} and a tetrahedral arrangement of hydrogen bonds. The collapse of this intermediate then produces the enzyme-acyl intermediate. The lysophospholipid is released by lateral diffusion in the membrane. The fatty acid product is released after a deacylation with water acting as the nucleophile by lateral diffusion into the mem-

brane or by the dissociation of the dimer [62]. The purpose of OmpLA is not fully clear yet. On the one hand the degradation of phospholipids in the outer leaflet of the outer membrane restores its integrity and mechanisms for the active uptake and recycling of the products have been published [20, 30, 31, 34, 46]. Also, in *Pseudomonas oleovorans* it has been shown that a periplasmic *cis-trans* isomerase acting on fatty acids can convert *cis*-double bonds into the *trans* conformation which would lead to a reduction of the membrane permeability and fluidity after reincorporation [52] thereby allowing OmpLA to act like a sensor for changes in the physical properties of the membrane [18]. On the other hand lysophospholipid and fatty acid products further destabilize the outer membrane due to their detergent-like properties thereby facilitating the semispecific excretion of colicins and other effector molecules [10, 14, 17, 44, 54, 63]. This implies, that OmpLA is also affecting the virulence of pathogens. The working principle of OmpLA is summarized in Figure 9.

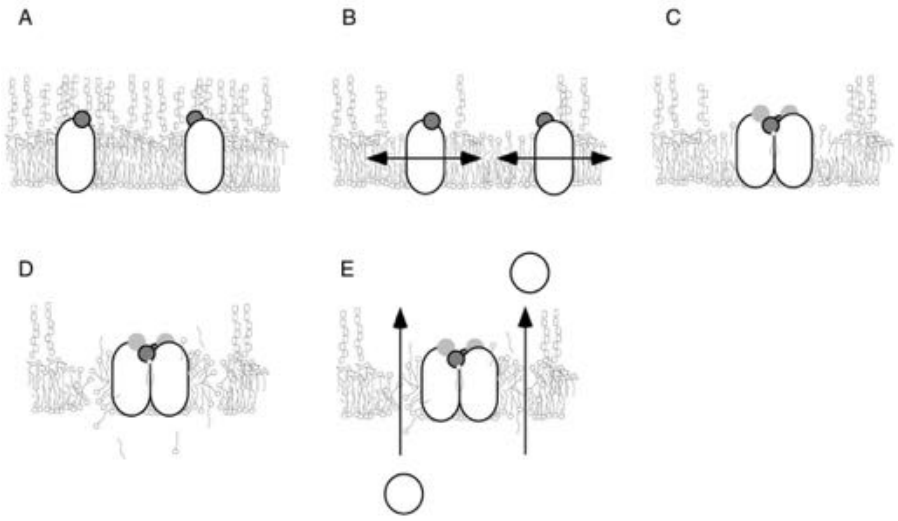

Figure 9: Working principle OmpLA. A) In an intact outer membrane with only LPS in the outer leaflet OmpLA is in its inactive monomeric form. B) Upon perturbations of the outer membrane phospholipids appearing in the outer leaflet. C) OmpLA forms dimers and in the active site Ca^{2+} and substrate are bound. D) After hydrolysis of the phospholipids the outer membrane is further destabilized. D) This facilitates the release of bacteriocins. Figure taken from Snijder et al. 2000 [62]

3 MATERIALS AND METHODS

In this chapter the materials and methods used during this project are presented. First, some information about the HS-AFM, the cantilevers and the chemicals are given. Second, the image processing is briefly described. The last part contains some workflow descriptions.

3.1 MATERIALS

3.1.1 *HS-AFM 1.0 - Ando Model*

The HS-AFM used in this project was the HS-AFM 1.0 - Ando model (RIBM, Japan). It was developed by Prof. Toshio Ando at the Kanazawa University in Japan and commercialized by RIBM. It is worldwide the first commercially available HS-AFM capable of imaging biological samples at video frame rate. The HS-AFM was operated in oscillating mode. The free amplitude was set to $\sim$ 1 nm and the imaging amplitude setpoint to $\sim 0.9 - 0.95$ nm. Like this, images ranging from 100×100 nm^2 up to 600×600 nm^2 with 200×200 to 300×300 pixels were recorded. In the following, the setup and particularly the scanner and cantilever holder are depicted (for more information see Section 2.1.3.)

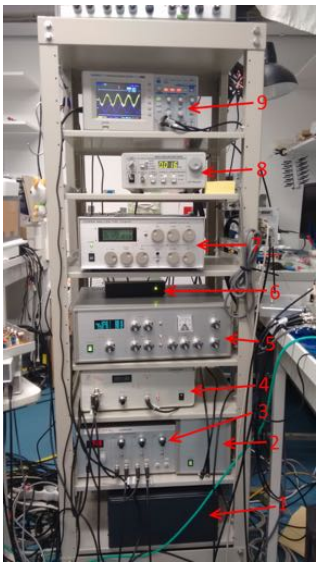

(a) 1) PCI slot extender; 2) Motor driver; 3) XY-Piezo driver; 4) Z-Piezo driver; 5) Feedback unit; 6) Q-controller 7) Fourier analyzer; 8) Power supply for LD; 9) Oscilloscope.

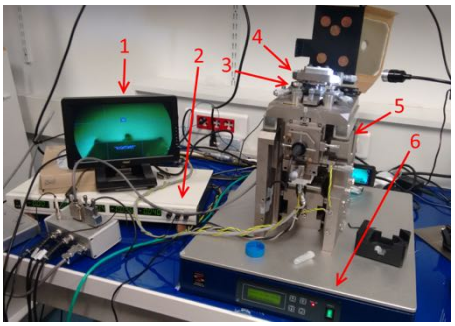

(b) 1) Monitor; 2) Signal processor; 3) Cantilever holder; 4) Scanner; 5) AFM Head; 6) Vibration-isolation table.

Figure 10: HS-AFM setup.

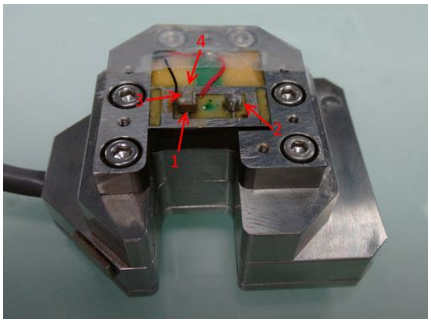

(a) Scanner. 1) Z-piezo; 2) Dummy Stage; 3) Glass rod; 4) Mica.

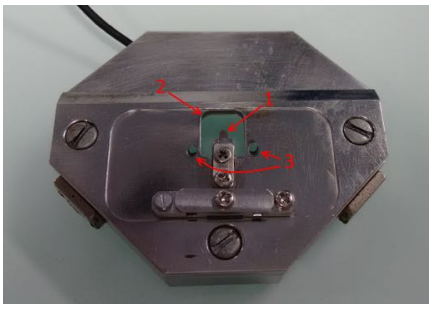

(b) Cantilever holder. 1) Cantilever; 2) Fluid cell; 3) Fluid in- and outlet.

Figure 11: Scanner (left) and cantilever holder (right).

3.1.2 *Cantilevers, Chemicals*

Chemicals of the highest available purity were purchased. Ethylenediaminetetraacetic acid (EDTA), NaCl, $MgCl_2$ and tris (hydroxymethyl) aminomethane (Tris) were from Sigma-Aldrich (Steinheim, Germany), $CaCl_2$ was from Carl Roth (Karlsruhe, Germany). Cantilevers used in this project were USC-F1.2-k0.15 (NanoWorld, Neuchâtel, Switzerland). These cantilevers are optimized for high speed scanning applications in liquid and the low force constant of 0.15 N/m makes them suitable for measuring biological samples. The cantilever is made of

a quartz-like material and has a 20 nm thick gold reflective coating on both sides of the probe (tip uncoated). The tip is made of wear resistant High Density Carbon/Diamond Like Carbon (HDC/DLC) material. Tip height: ~ 2.5 µm, radius of curvature: < 10 nm, tip aspect ratio: ~ 5 : 1, tilt compensation: 8°. The cantilever properties can be seen in Table 1. SEM images of the cantilever and its tip are depicted in Figure 12.

Type	USC-F1.2-k0.15
Resonance Frequency	1.2 MHz (air), 0.6 MHz (liquid)
Force Constant	0.15 N/m
Quality factor	~2
Cantilever length	7 µm
Cantilever width	2 µm
Cantilever thickness	0.08 µm

Table 1: Cantilever properties.

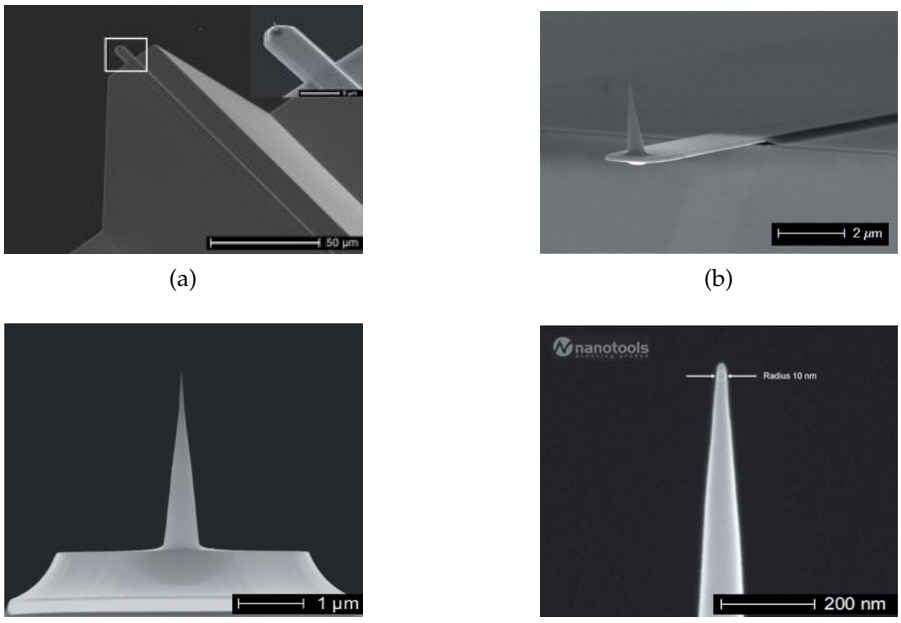

(a) (b) (c) (d)

Figure 12: SEM images of an ultra-short cantilever USC-F1.2-k0.15 (NanoWorld, Neuchâtel, Switzerland) and its tip. The white frame in picture (a) indicates the area of the closeup in the top right corner. Images taken from nanoworld.com.

3.1.3 *Additional Devices*

For gradual exchange of buffer during HS-AFM measurements, a pumping system (PHD ULTRA model PP PRO6, Harvard Apparatus, USA) was used (see Section 3.3.3). After imaging the cantilever tips were cleaned by a plasma cleaner (ZEPTO version B, Diener electronic, Germany) (Section 3.3.4).

3.2 DATA ANALYSIS

The HS-AFM pictures were processed using ImageJ 1.51d in the following way:

- First-order flattening
- Contrast adjustment
- Drift correction with frame-to-frame cross-correlation using the lab-made VideoJ 0.3 ImageJ plug-in [25][37].

3.3 EXPERIMENTAL METHODS

3.3.1 *HS-AFM Imaging*

Before imaging, the HS-AFM needs to be set up in the following way:

- Clean cantilever holder.
- Mount clean cantilever.
- Fill fluid cell (~100µl).
- Adjust laser.
  - Set camera on night view.
  - Focus on cantilever.
  - Adjust x, y, z and tilt of the cantilever to bring sum to maximum and difference to 0.
  - Optional: Adjust laser power by altering the current (about 0.016-0.02 mA).
  - Perform a frequency sweep and check cantilever response.
- Glue glass rod to the Z-piezo with nail polish (see Figure 13)
- Glue mica disc on the glass rod with superglue (see Figure 13)
- Incubate sample as described in Section 3.3.2.
- Mount scanner (Don't crash into cantilever) and check if the appropriate Q-Box is installed.

- Align cantilever over sample.
- Set gain and ω gain.
- Adjust frequency by checking amplitude on feedback controller (Amplitude should be ~500 mV, maybe adjust the gains).
- Turn on xy-scanner, z-scanner and feedback controller (Hear if z-scanner is making noise$\longrightarrow$if yes: abort and check if there is too much liquid in the fluid cell).
- Set setpoint to $\sim 0.9 - 0.95$ and do approach.
- Start scanning.
- Lower setpoint to an appropriate level.
- Adjust tilt.

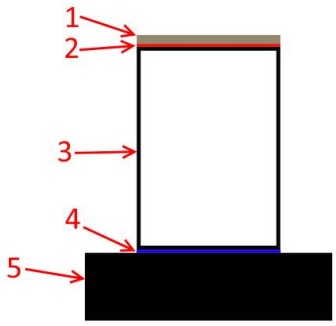

Figure 13: 1) Mica; 2) Superglue; 3) Glass rod; 4) Nail polish 5) Z-piezo.

3.3.2 *Sample Preparation*

Before measuring, the sample was prepared in the following manner:

- Cleave mica disc with scotch tape.
- Apply $1 - 2$ µl of the sample on the mica (see. Figure 14).
- Cover the mica with a humid chamber to avoid drying.
- Incubate the sample for 10 min.
- Remove excess sample by adding a droplet of buffer on the mica and remove it with a twisted tissue. Repeat this rinsing process 10 times.

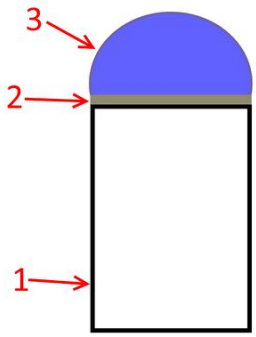

Figure 14: Sample incubation (Side view). 1) Glass rod; 2) Mica; 3) Sample ($1-2$ µl).

3.3.3 *Pumping System*

A high-precision pump (PHD ULTRA model PP PRO6, Harvard Apparatus, USA) was used in some experiments to exchange a starting buffer with an exchange buffer during AFM measurements at a flow speed of 10 µl/min. Therefore, two syringes with attached tubes were mounted on opposite sides of the pump, one for pumping and the other one for drawing. The previously washed tubes were then connected to the in- and the outlet of the cantilever holder (see Figure 11). The inlet tube filled with the exchange buffer had to have a small air bubble right at the inlet of the cantilever holder in order to avoid diffusion before pumping. A small hole had to be cut on the upper side of the tube to avoid pumping the air bubble into the fluid cell. The outlet tube partially filled with water contained a small volume of starting buffer separated by an air bubble from the water right at the outlet of the cantilever holder in order to avoid undesired diffusion.

Figure 15: Pumping system connected to the cantilever holder. Picture taken from Miyagi et al. 2016 [49].

3.3.4 *Tip Cleaning*

To clean the cantilever tips from scanning residues, they were treated in the following way. This process led to clean tips in the majority of

cases. Sometimes the tips were even sharpened by the plasma. In rare cases, the tip or the cantilever were destroyed. The plasma cleaner used during this project is depicted in Figure 16.

- Submerge cantilever in Alconox (Alconox, New York, USA) for several minutes.
- Submerge cantilever in Milli-Q Water for at least 10 min.
- Put the cantilever into He-Plasma (0.3 mbar, 40 kHz, 120 W) for 80 s.

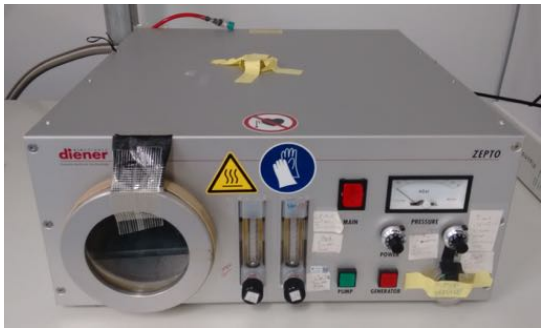

Figure 16: Plasma cleaner ZEPTO version B (Diener electronic, Ebhausen, Germany).

4

RESULTS AND DISCUSSION

In the following chapter the results of the HS-AFM measurements of OmpLA are presented. To study the structure-function relationship of OmpLA and elucidate the dynamics of the protein working mechanisms we performed HS-AFM imaging of OmpLA reconstituted in lipid bilayers before, during and after the activation by calcium. In the first section it is shown that the addition of Ca^{2+} triggers a gradual membrane degradation. This finding is confirmed by several control experiments that are presented in part Section 4.2 and Section 4.3. Here, a mock sample of DLPC membranes without proteins were imaged upon addition of Ca^{2+}. After 2 hours of constant imaging no degradation was detected implying that the membrane shrinking is induced specifically by OmpLA. Neither probable charging effects of calcium nor the imaging process of the HS-AFM destroy the membranes. In addition, it is shown that the presence of Mg^{2+} does not trigger any membrane degradation indicating that the observed process and OmpLA is highly specific to Ca^{2+}. In Section 4.4, the effect of different lipids to OmpLA was tested. In contrast to DLPC membranes, the reconstitution of OmpLA in POPC resulted in densely packed lipid patches and protein crystals in different configurations. Furthermore, in the last part of this chapter the incorporation of OmpLA into DLPC bilayers, was studied. To this goal, OmpLA solubilized in F_6OPC, a surfactant, was added to DLPC bilayers and the incorporation of the folded OmpLA into lipid bilayers was monitored. Unless otherwise stated, all experiments were performed in standard buffer (300 mM NaCl, 20 mM Tris, 2 mM EDTA, pH 7.4) and recorded with an image-acquisition rate of 1 frame per second.

.

4.1 MEMBRANE DEGRADATION

OmpLA reconsituted in DLPC was imaged in standard buffer containing EDTA in order to prevent dimerization due to calcium and subsequent activation of the protein. In presence of 2 mM EDTA some undefined structures protruding about 1.6 nm out of the membrane were observed (Figure 17, upper panel second picture; Figure 18). The addition of 2.5 mM (total) Ca^{2+} caused immediately a topographical change allowing the clear detection of individual molecules diffusing in the membrane (Figure 17, upper panel, 3^{rd} picture). The protrusion height of the molecules was about $1.6 - 1.7$ nm (Figure 19). The change in appearance was reversible by the addition of EDTA

(s. Section A.2). This effect certainly is an electrostatic shielding effect and is not related to the function of the protein. Over time, the membrane started shrinking and detaching from the mica support until only thin tubular patches with densely packed proteins remained (Figure 17). The timescale of this shrinking process (from first Ca^{2+} addition to tubular structures) varied from about 30 to 90 minutes. It started slowly and accelerated over time. Figure 20 shows high-resolution HS-AFM snapshots of the shrinking process. Within 3 minutes a membrane of about 20,000 nm^2 was degraded to a densly packed OmpLA patch of about 7000 nm^2. In this OmpLA crystal individual dimers could be visualized, partially already in the isolated state.

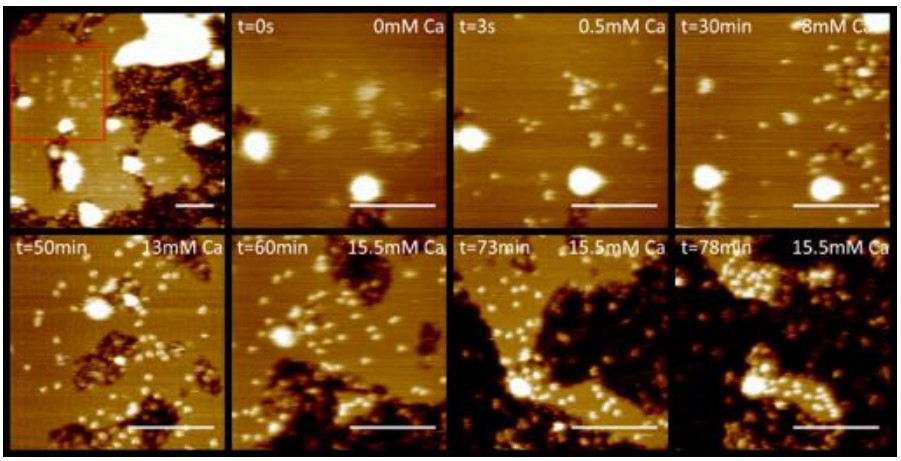

Figure 17: Ca^{2+} induced OmpLA activation. The red frame in the first image indicates the area imaged in the subsequent pictures. T=0 s corresponds to the last frame before the addition of Ca^{2+}. Right after this addition, the vague protrusions in the membrane became well defined structures (t=3 s). The proteins then diffuse in the bilayer and destabilize it over time. In the end, tube like structures with densely packed OmpLA can be observed. Scale bar: 100 nm. Full-color scale: 6 nm.

To trigger OmpLA activation by Ca^{2+}, 5 µl of 50 mM Ca^{2+} was pipetted directly into the buffer bath while imaging (Figure 17 and Figure 20). Alternatively, to avoid huge perturbations during the imaging process like imaging-amplitude fluctuations or scanning position loss, a pumping system can be used. With this system buffer can be simultaneously removed and replaced with a Ca^{2+} containing buffer leading to a smoother increase in the Ca^{2+} concentration compared to the pipetting method. By gradually removing EDTA and continuously adding Ca^{2+} using this buffer exchanging system the same mechanism of membrane degradation was observed (Figure 21). Furthermore, the defined pumping rate of the buffer exchanging system allows an estimation of Ca^{2+} concentration at each timepoint (Figure 22). It is noteworthy, that the starting buffer in the pumping

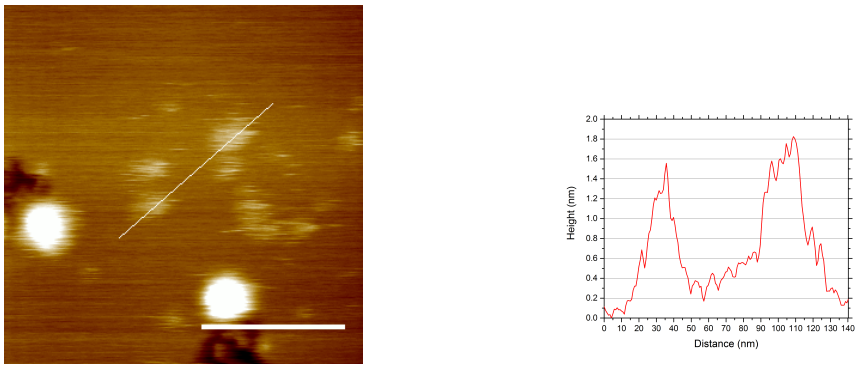

(a) (b)

Figure 18: OmpLA in presence EDTA. Cross-section analysis. The vague protrusions are about 1.6 nm in height. Scale bar: 100 nm. Full-color scale: 6 nm.

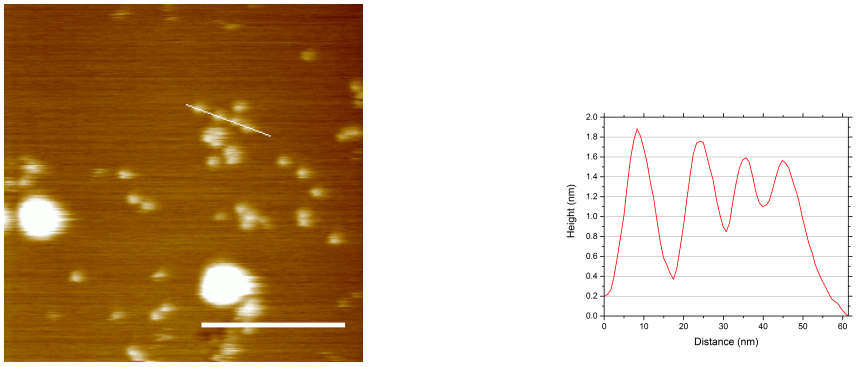

(a) (b)

Figure 19: OmpLA in presence of Ca. Cross-section analysis. The protein structures are about $1.6 - 1.7$ nm in height. Compared to OmpLA in presence EDTA there is no significant change in height. Scale bar: 100 nm. Full-color scale: 6 nm.

system experiment did not contain NaCl. The opening process between the first and the second picture of Figure 21 is described in Section A.1.

To exclude that the membrane degradation is caused by the HS-AFM tip scanning different sample positions were imaged that were not scanned with the tip before. Figure 23 shows several degraded OmpLA membrane patches in imaged (indicated by a square) and non-imaged areas, thereby excluding any membrane destruction by tip-sample interactions.

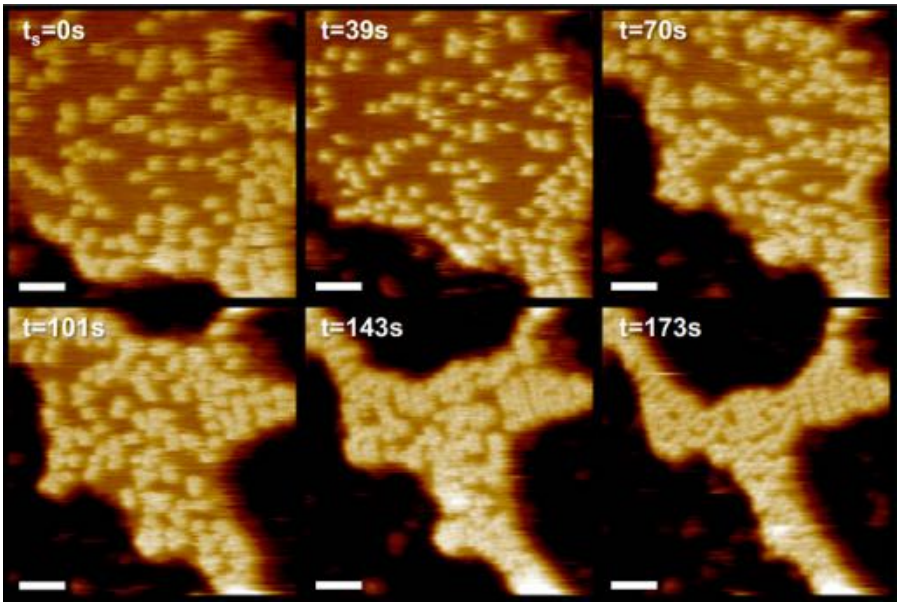

Figure 20: High resolution HS images of the OmpLA induced membrane degradation. This patch with already densely packed OmpLA was found 76 min after the first addition of Ca^{2+} (t=0 s). The bilayer was then degraded within only 3 min forming densely packed almost crystalline tube like structures. In the last picture (t=173 s) some substructures of OmpLA can be seen, maybe corresponding to the OmpLA dimer interface. Scale bar: 25 nm. Full-color scale: 6 nm.

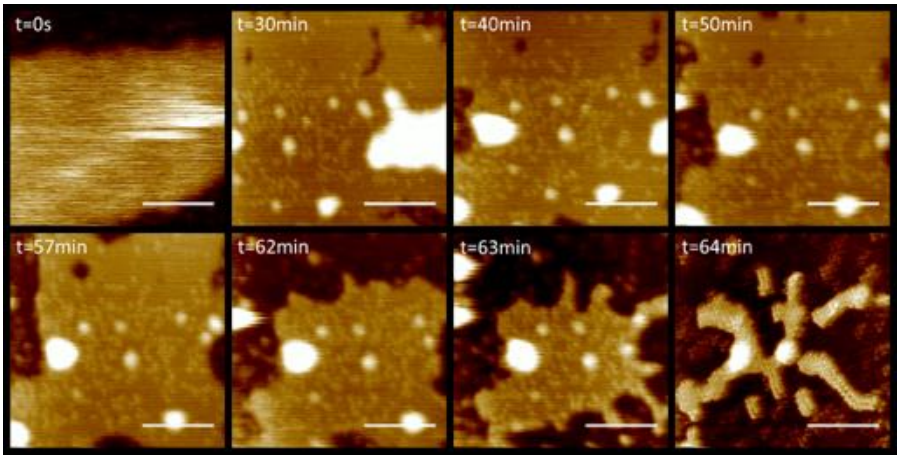

Figure 21: Observation of the OmpLA membrane degrations using a gradual buffer exchanging system. Exchange from 20 mM Tris, 2mM EDTA to 20 mM Tris, 2 mM Ca. Scale bar: 100 nm. Full-color scale: 9 nm.

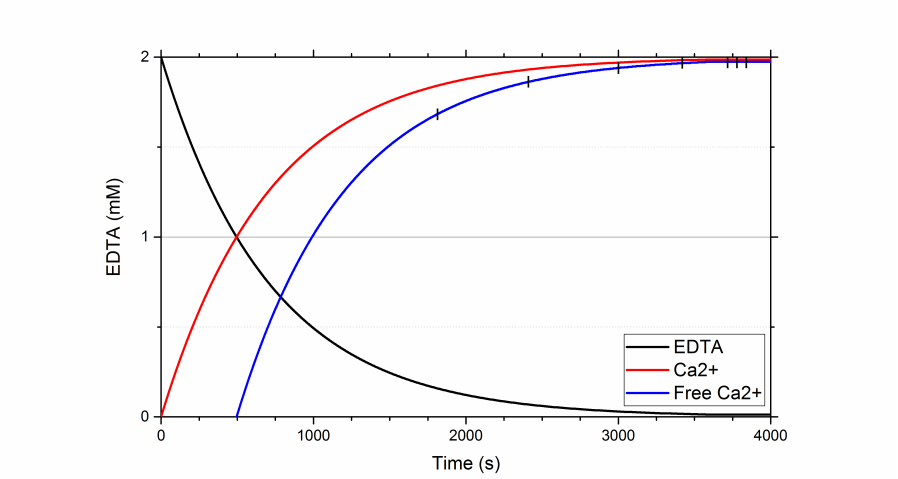

Figure 22: Graph belonging to the pumping experiment in Figure 21. A starting buffer (20 mM Tris, 2 mM EDTA, pH 7.4) is replaced by an exchange buffer (20 mM Tris, 2 mM EDTA, 2 mM $CaCl_2$, pH 7.4) at a flow rate of 10 µl/min. The black line corresponds to the EDTA concentration in the fluid cell of the HS-AFM, the red one to the Ca^{2+} concentration and the blue one to the concentration of free Ca^{2+}-ions if all the EDTA is bound. The black markers on the blue line indicate the points in time of the pictures in Figure 21. This model implies instantaneous mixing in the fluid cell of the HS-AFM which leads to an inherent error for the calculated concentrations. Nevertheless, it allows to roughly estimate the current concentrations during an experiment.

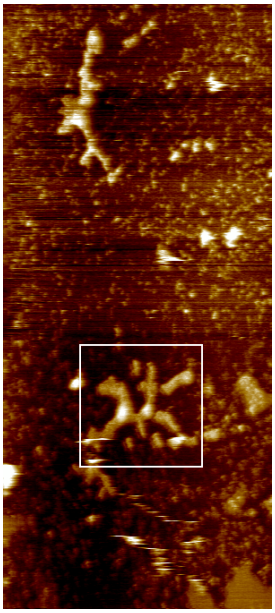

Figure 23: The white frame indicates the scan area of Figure 21. On the top part of the picture it can be seen, that the membrane was also shrinking beside the scan area forming again tubular structures densely packed with OmpLA. Total width of the picture: 600 nm.

4.2 MEMBRANE DEGRADATION IS PROTEIN-INDUCED

In order to check if the membrane degradation described in the previous section is induced by OmpLA and to exclude other effects like destructive tip-sample interaction or charging effects by the addition of Ca^{2+}, experiments with a mock sample were performed. For this, DLPC membranes without the protein were studied in absence and presence of Ca^{2+}, similar to the previously described experiments. As demonstrated in the following Figure 24 no significant membrane degradation was detected upon Ca^{2+} addition, indicating that OmpLA is responsible for the destabilization and subsequent degradation of the membrane.

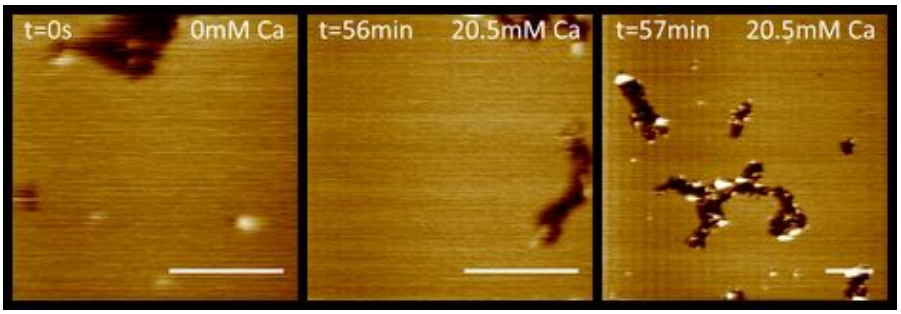

Figure 24: Bare DLPC membrane in absence and presence of Ca^{2+}. No degradation of lipid patches without protein upon the addition of Ca^{2+} could be observed with Ca^{2+} concentrations up to 20.5 mM within a timeframe of 57 minutes. Scale bar: 100 nm. Full-color scale: 4.5 nm.

4.3 MEMBRANE DEGRADATION IS CALCIUM-DEPENDENT

OmpLA is known to be highly specific to Ca^{2+}. Accordingly, to test if the membrane degradation process can be triggered by other divalent cations, and thus exclude charging artefacts the experiments were repeated with magnesium instead of calcium. As shown in the following Figure 25a the membrane is not affected by the addition of magnesium even after an imaging period for more than 2 hours. In contrast however, the subsequent addition of calcium yielded in a membrane shrinking and a complete degradation within 40 minutes (see Figure 25b), indicating that the process is really driven by the Ca^{2+} activated protein. Notably, the change in appearance, from vague protrusions in EDTA to well defined structures in presence of Ca^{2+} in the membrane, was also observed by the addition of Mg^{2+} implying that this topographical change is a charging artefact in the tip-sample interaction.

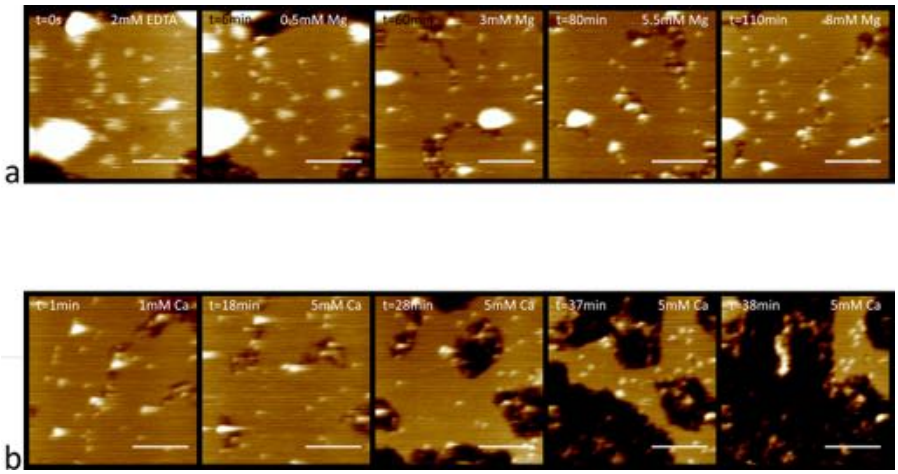

Figure 25: Membrane degradation is Ca^{2+} specific. a) Mg^{2+} was added stepwise up to a final concentration of 10 mM (first row, data for 10 mM not shown). The same change in appearance of the protein as with the addition of Ca^{2+} was observed (compare picture t=0 and subsequent pictures). No signs of membrane degradation were detected two hours after the first addition of Mg^{2+}. b) Subsequently, Ca^{2+} was added stepwise up to a concentration of 5 mM triggering again the membrane degradation process (second row). Scale bar: 100 nm. Full-color scale: 4 nm.

4.4 OMPLA ALIGNMENT LIPID-DEPENDENT

The effect of the lipid type on OmpLA and its function was tested by OmpLA reconstitutions in POPC lipids. The main difference of the previously described DLPC membranes and POPC membranes is that POPC has longer hydrophobic tails and therefore forms membranes with a broader hydrophobic region (DLPC ~ 2 nm vs. POPC ~ 2.9 nm). For HS-AFM experiments these OmpLA-POPC membranes were freshly adsorbed and imaged in standard buffer like the DLPC membranes described in Section 4.1. In POPC lipid however, OmpLA was already observed in stable, well-defined structures in Ca^{2+}-free condition (2 mM EDTA) either aligned in regular crystals (Figure 26a and Figure 27a) or densely packed (Figure 28). The different crystal alignments found (compare Figure 26a and Figure 27a) showed a nearly identical periodicity along the proteins (4.8 nm vs. 4.75 nm) as well as perpendicular to the proteins (10.4 nm vs. 10.75) but with an inverse height distribution. These two forms of OmpLA crystal symmetries may correspond to the two protein faces or alternatively, to OmpLA monomer and dimer alignments, respectively. Interestingly, Figure 27 also shows some ring-like structures on the borders of the crystal.

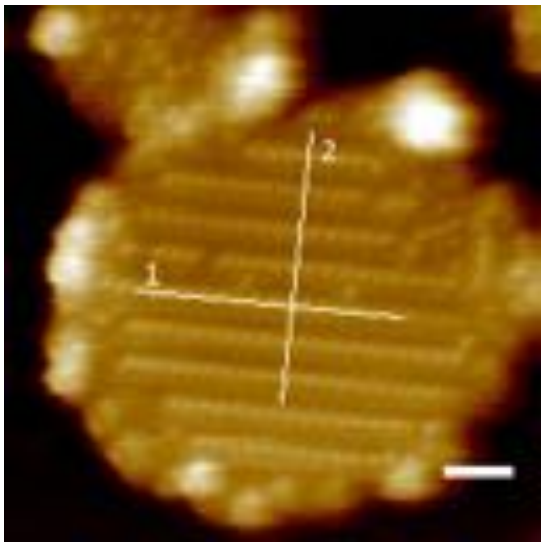

(a) OmpLA crystal reconstituted in POPC membranes. Scale bar: 20 nm. Full-color scale: 11 nm.

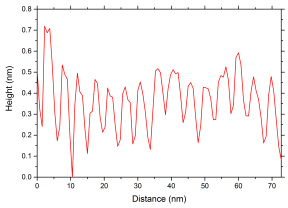

(b) Line 1

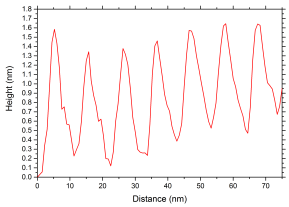

(c) Line 2

Figure 26: Peak to peak distance along the proteins (line 1): 4.8 nm. Peak to peak distance perpendicular to the proteins (line 2): 10.4 nm.

Ca^{2+} was added into the measuring buffer, similar to the experiments described in Section 4.1. In contrast to OmpLA reconstituted in DLPC, neither membrane shrinking or degradation nor a significant change in the protein structure or assembly was observed within a timeframe of about 45 minutes (Figure 28). This may be due to the dense packing of OmpLA which is similar to the dense packing observed before in DLPC however without a tubular structure of the membrane.

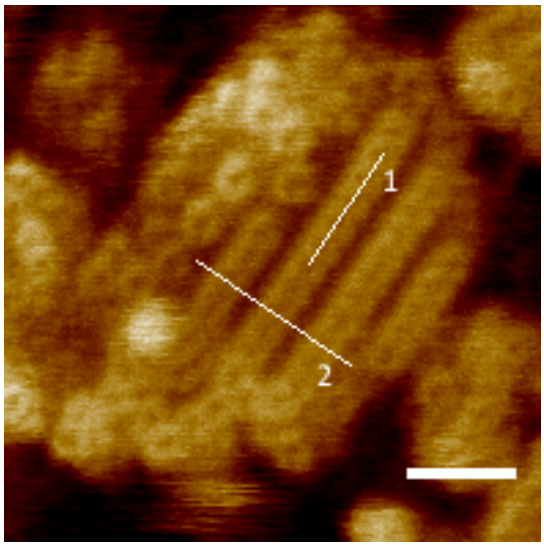

(a) OmpLA crystal reconstituted in POPC membranes. Scale bar: 20 nm. Full-color scale: 5 nm.

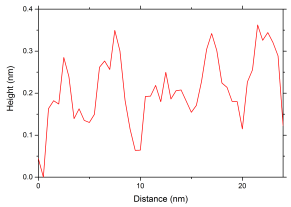

(b) Line 1

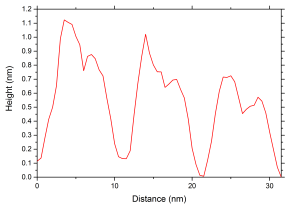

(c) Line 2

Figure 27: Peak to peak distance along the proteins (line 1): 4.75 nm. Peak to peak distance perpendicular to the proteins (line 2): 10.75 nm.

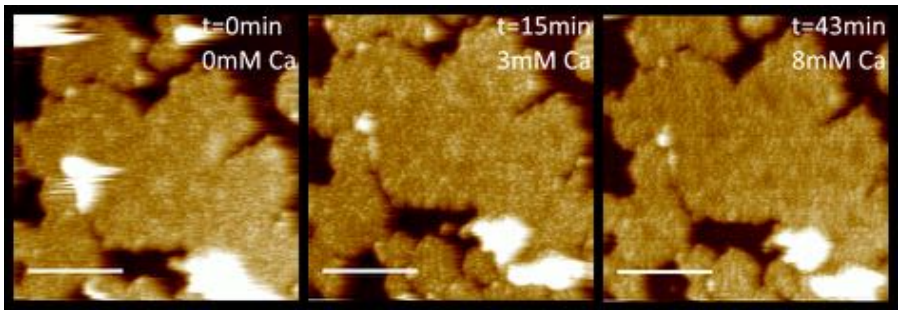

Figure 28: Beside crystals, densely packed OmpLA membranes were found in the POPC sample. Similar to the experiments with DLPC, Ca^{2+} was added stepwise to the buffer up to a final concentration of 8 mM but no degradation of the membrane was detected.

4.5 OMPLA INTEGRATION INTO DLPC

To elucidate if it is possible to incorporate already folded OmpLA into lipid membranes and to study the whole embedding process HS-AFM was used to directly visualize the insertion process of OmpLA

from micelles into lipid membranes. In a study from Frotscher et al. [26, 27] it was shown that the detergent F_6OPC does not drastically affect lipid membranes and that OmpLA in F_6OPC micelles could successfully be integrated in liposomes. Accordingly, OmpLA solubilized in F_6OPC (2.244 mg/ml) was added to DLPC bilayers on mica support. After a time-window between 20-70 minutes the insertion of OmpLA into the bilayers was observed (Figure 29 and Figure 30).
In Figure 29 9 µl of OmpLA in F_6OPC were added stepwise into standard buffer charged with 20.5 mM Ca^{2+}. 18 min after the first respectively 260 s after the last addition the first proteins appeared in the membrane. Because the amplitude of the cantilever was highly decreased when the process started, no pictures are available from the beginning. After the integration was initiated, it continued rapidly, yielding lipid bilayers with crowded OmpLA within seconds.

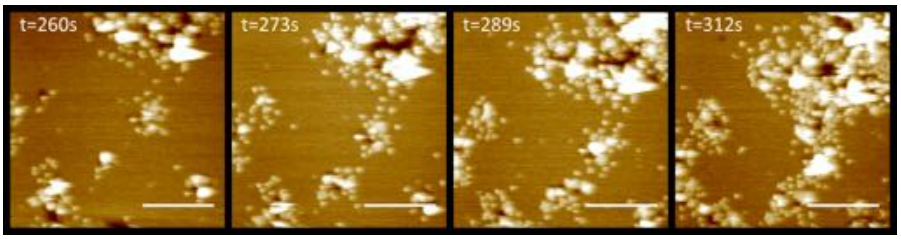

Figure 29: OmpLA integration into DLPC bilayer. Scale bar: 100 nm. Full-color scale: 7 nm.

In Figure 30 10 µl of OmpLA in F_6OPC were added stepwise into standard buffer charged with 10 mM Ca^{2+}. 71 min after the first respectively 18 min after the last addition first proteins appeared in the membrane. 25 min after the last addition, the process speeded up drastically, yielding again lipid bilayers with crowded OmpLA.

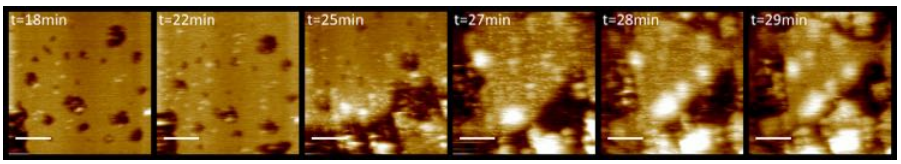

Figure 30: OmpLA integration into DLPC bilayer. Scale bar: 100 nm. Full-color scale: 7 nm.

After the process stabilized within 30 minutes densely packed OmpLA membrane patches were observed (Figure 31). OmpLA is forming nearly crystalline structures upon integration in the membrane within minutes. But, due to the complete overload of protein, these are just partially observable.

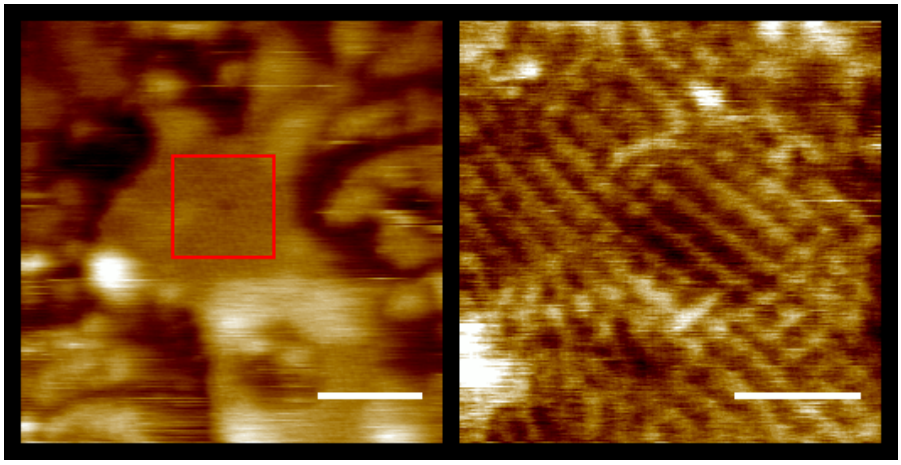

Figure 31: Close-up view of a different area of the sample. The red frame in the left picture indicates the position of the right picture. Scale bar: 100 nm (left) and 30 nm (right). Full-color scale: 7 nm.

5 CONCLUSION

In this project, we used high speed atomic force microscopy (HS-AFM) to visualize the dynamics and activity of OmpLA upon activation triggered by the presence of phospholipids and calcium. Like this we were able to monitor the OmpLA induced and calcium dependent shrinking of DLPC lipid bilayers in real time with nanometer resolution.
It was shown that OmpLA is degrading and destabilizing the lipid bilayers leading to shrinking of the lipid patches (see Figure 17, Figure 20 and Figure 21) until densely packed, crystal-like patches were present (see Figure 20). These results were confirmed by several control experiments showing that the shrinking process was indeed depending on OmpLA (see Figure 24), was not triggered by other charges and is highly specific for calcium (see Figure 25), and was not triggered by the tip scanning process as even un-scanned areas were affected (see Figure 23). Investigations of OmpLA reconstituted in POPC instead of DLPC revealed OmpLA crystals in different alignments (see Figure 26 and Figure 27) or in densely packed patches (see Figure 28). The addition of calcium did not trigger any degradation of the lipid patches presumably because of the dense packing which resembles the dense packing found in DLPC membranes after the shrinking process finished. Another experiment with OmpLA solubilized in F_6OPC micelles demonstrated that OmpLA can be inserted into lipid bilayers in a folded state (see Figure 29, Figure 30 and Figure 31).

BIBLIOGRAPHY

[1] T. Ando, N. Kodera, E. Takai, D. Maruyama, K. Saito, and A. Toda. "A high-speed atomic force microscope for studying biological macromolecules." In: *Proceedings of the National Academy of Sciences of the United States of America* 98.22 (2001), pp. 12468–12472. DOI: 10.1073/pnas.211400898.

[2] Toshio Ando, Takayuki Uchihashi, and Takeshi Fukuma. "High-speed atomic force microscopy for nano-visualization of dynamic biomolecular processes." In: *Progress in Surface Science* 83.7–9 (2008), pp. 337–437. DOI: 10.1016/j.progsurf.2008.09.001.

[3] Toshio Ando, Takayuki Uchihashi, and Noriyuki Kodera. "High-Speed AFM and Applications to Biomolecular Systems." In: *Annual Review of Biophysics* 42.1 (2013), pp. 393–414. DOI: 10.1146/annurev-biophys-083012-130324.

[4] Toshio Ando, Takayuki Uchihashi, and Simon Scheuring. "Filming Biomolecular Processes by High-Speed Atomic Force Microscopy." In: *Chemical Reviews* 114.6 (2014), pp. 3120–3188. DOI: 10.1021/cr4003837.

[5] Toshio Ando, Noriyuki Kodera, Takayuki Uchihashi, Atsushi Miyagi, Ryo Nakakita, Hayato Yamashita, and Keiko Matada. "High-speed Atomic Force Microscopy for Capturing Dynamic Behavior of Protein Molecules at Work." In: *e-Journal of Surface Science and Nanotechnology* 3 (2005), pp. 384–392. DOI: 10.1380/ejssnt.2005.384.

[6] Toshio Ando, Takayuki Uchihashi, Noriyuki Kodera, Daisuke Yamamoto, Atsushi Miyagi, Masaaki Taniguchi, and Hayato Yamashita. "High-speed AFM and nano-visualization of biomolecular processes." In: *Pflügers Archiv - European Journal of Physiology* 456.1 (2007), pp. 211–225. DOI: 10.1007/s00424-007-0406-0.

[7] R. C. Barrett and C. F. Quate. "High-speed, large-scale imaging with the atomic force microscope." In: *Journal of Vacuum Science & Technology B* 9.2 (1991), pp. 302–306. DOI: 10.1116/1.585610.

[8] G. Binnig, C. F. Quate, and Ch. Gerber. "Atomic Force Microscope." In: *Phys. Rev. Lett.* 56 (1986), pp. 930–933. DOI: 10.1103/PhysRevLett.56.930.

[9] G. Binnig, H. Rohrer, Ch. Gerber, and E. Weibel. "Surface Studies by Scanning Tunneling Microscopy." In: *Phys. Rev. Lett.* 49 (1982), pp. 57–61. DOI: 10.1103/PhysRevLett.49.57.

[10] Russell E. Bishop. "Structural biology of membrane-intrinsic β-barrel enzymes: Sentinels of the bacterial outer membrane." In: *Biochimica et Biophysica Acta (BBA) - Biomembranes* 1778.9 (2008), pp. 1881–1896. DOI: 10.1016/j.bbamem.2007.07.021.

[11] Ronald G. P. M. Brok, Nick Dekker, Nathalie Gerrits, Hubertus M. Verheij, and Jan Tommassen. "A Conserved Histidine Residue of Escherichia Coli Outer-Membrane Phospholipase A is Important for Activity." In: *European Journal of Biochemistry* 234.3 (1995), pp. 934–938. DOI: 10.1111/j.1432-1033.1995.934_a.x.

[12] Ignacio Casuso, Felix Rico, and Simon Scheuring. "High-speed atomic force microscopy: Structure and dynamics of single proteins." In: *Current Opinion in Chemical Biology* 15.5 (2011), pp. 704–709. DOI: 10.1016/j.cbpa.2011.05.007.

[13] Ignacio Casuso, Jonathan Khao, Mohamed Chami, Perrine Paul-Gilloteaux, Mohamed Husain, Jean-Pierre Duneau, Henning Stahlberg, James N. Sturgis, and Simon Scheuring. "Characterization of the motion of membrane proteins using high-speed atomic force microscopy." In: *Nature Nanotechnology* 7.8 (2012), pp. 525–529. DOI: 10.1038/nnano.2012.109.

[14] D. Cavard, D. Baty, S. P. Howard, H. M. Verheij, and C. Lazdunski. "Lipoprotein nature of the colicin A lysis protein: effect of amino acid substitutions at the site of modification and processing." In: *Journal of Bacteriology* 169.5 (1987), pp. 2187–2194.

[15] Nicolas Chiaruttini, Lorena Redondo-Morata, Adai Colom, Frédéric Humbert, Martin Lenz, Simon Scheuring, and Aurélien Roux. "Relaxation of Loaded ESCRT-III Spiral Springs Drives Membrane Deformation." In: *Cell* 163.4 (2015), pp. 866–879. DOI: 10.1016/j.cell.2015.10.017.

[16] John E. Cronan and Daniel L. Wulff. "A role for phospholipid hydrolysis in the lysis of Escherichia coli infected with bacteriophage T4." In: *Virology* 38.2 (1969).

[17] N. Dekker, J. Tommassen, and H. M. Verheij. "Bacteriocin release protein triggers dimerization of outer membrane phospholipase A in vivo." In: *Journal of Bacteriology* 181.10 (1999), pp. 3281–3283.

[18] Niek Dekker. "Outer-membrane phospholipase A: known structure, unknown biological function." In: *Molecular microbiology* 35.4 (2000), pp. 711–717.

[19] Niek Dekker, Jan Tommassen, Ariel Lustig, Jürg P. Rosenbusch, and Hubertus M. Verheij. "Dimerization regulates the enzymatic activity of Escherichia coli outer membrane phospholipase A." In: *Journal of Biological Chemistry* 272.6 (1997), pp. 3179–3184.

[20] Concetta C. Dirusso and Paul N. Black. "Bacterial long chain fatty acid transport: gateway to a fatty acid-responsive signaling system." In: *The Journal of Biological Chemistry* 279.48 (2004), pp. 49563–49566. DOI: 10.1074/jbc.R400026200.

[21] Guy Dodson and Alexander Wlodawer. "Catalytic triads and their relatives." In: *Trends in Biochemical Sciences* 23.9 (1998), pp. 347–352. DOI: 10.1016/S0968-0004(98)01254-7.

[22] Allison Doerr. "Membrane protein structures." In: *Nature Methods* 6.1 (2009), pp. 35–35. DOI: 10.1038/nmeth.f.240.

[23] Georg E. Fantner, Paul Hegarty, Johannes H. Kindt, Georg Schitter, Geraldo A. G. Cidade, and Paul K. Hansma. "Data acquisition system for high speed atomic force microscopy." In: *Review of Scientific Instruments* 76.2 (2005), p. 026118. DOI: 10.1063/1.1850651.

[24] Georg E. Fantner et al. "Components for high speed atomic force microscopy." In: *Ultramicroscopy* 106.8–9 (2006), pp. 881–887. DOI: 10.1016/j.ultramic.2006.01.015.

[25] Peter Fechner, Thomas Boudier, Stéphanie Mangenot, Szymon Jaroslawski, James N. Sturgis, and Simon Scheuring. "Structural Information, Resolution, and Noise in High-Resolution Atomic Force Microscopy Topographs." In: *Biophysical Journal* 96.9 (2009), pp. 3822–3831. DOI: 10.1016/j.bpj.2009.02.011.

[26] Erik Frotscher, Bartholomäus Danielczak, Carolyn Vargas, Annette Meister, Grégory Durand, and Sandro Keller. "A fluorinated detergent for membrane-protein applications." In: *Angewandte Chemie (International Ed. in English)* 54.17 (2015), pp. 5069–5073. DOI: 10.1002/anie.201412359.

[27] Erik Frotscher, Bartholomäus Danielczak, Carolyn Vargas, Annette Meister, Grégory Durand, and Sandro Keller. "Ein fluoriertes Detergens für Membranprotein-Anwendungen." In: *Angewandte Chemie* 127 (2015), pp. 5158–5162. DOI: 10.1002/ange.201412359.

[28] P. de Geus, I. van Die, H. Bergmans, J. Tommassen, and G. de Haas. "Molecular cloning of pldA, the structural gene for outer membrane phospholipase of E. coli K12." In: *Molecular & general genetics: MGG* 190.1 (1983), pp. 150–155.

[29] K. L. Hardaway and C. S. Buller. "Effect of ethylenediaminetetraacetate on phospholipids and outer membrane function in Escherichia coli." In: *Journal of Bacteriology* 137.1 (1979), pp. 62–68.

[30] P. Hellion, F. Landry, P. V. Subbaiah, and P. Proulx. "The uptake and acylation of exogenous lysophosphatidylethanolamine by Escherichia coli cells." In: *Canadian Journal of Biochemistry* 58.12 (1980), pp. 1381–1386.

[31] H. Homma, M. Nishijima, T. Kobayashi, H. Okuyama, and S. Nojima. "Incorporation and metabolism of 2-acyl lysophospholipids by Escherichia coli." In: *Biochimica Et Biophysica Acta* 663 (1981), pp. 1–13.

[32] Anton J. G. Horrevoets, Hubertus M. Verheij, and Gerard H. de HAAS. "Inactivation of Escherichia coli outer-membrane phospholipase A by the affinity label hexadecanesulfonyl fluoride." In: *European Journal of Biochemistry* 198.1 (1991), pp. 247–253. DOI: 10.1111/j.1432-1033.1991.tb16008.x.

[33] Anton JG Horrevoets, Tilman M. Hackeng, Hubertus M. Verheij, Ruud Dijkman, and Gerard H. De Haas. "Kinetic characterization of Escherichia coli outer membrane phospholipase A using mixed detergent-lipid micelles." In: *Biochemistry* 28.3 (1989), pp. 1139–1147.

[34] L Hsu, S Jackowski, and C O Rock. "Uptake and acylation of 2-acyl-lysophospholipids by Escherichia coli." In: *Journal of Bacteriology* 171.2 (1989), pp. 1203–1205.

[35] A. D. L. Humphris, M. J. Miles, and J. K. Hobbs. "A mechanical microscope: High-speed atomic force microscopy." In: *Applied Physics Letters* 86.3 (2005), p. 034106. DOI: 10.1063/1.1855407.

[36] Mohamed Husain. "High speed atomic force microscopy for the study of structure and dynamics of membrane proteins." PhD thesis. Pierre-and-Marie-Curie University, 2012.

[37] Mohamed Husain, Thomas Boudier, Perrine Paul-Gilloteaux, Ignacio Casuso, and Simon Scheuring. "Software for drift compensation, particle tracking and particle analysis of high-speed atomic force microscopy image series: SOFTWARE FOR HIGH-SPEED ATOMIC FORCE MICROSCOPY IMAGE SERIES." In: *Journal of Molecular Recognition* 25.5 (2012), pp. 292–298. DOI: 10.1002/jmr.2187.

[38] Fabian Kebbel. "Structural and Functional Characterization of the Integral Membrane Proteins CitS and CCR5 by Electron Microscopy." PhD thesis. University of Basel, 2013.

[39] Johannes H Kindt, Georg E Fantner, Jackie A Cutroni, and Paul K Hansma. "Rigid design of fast scanning probe microscopes using finite element analysis." In: *Ultramicroscopy* 100.3–4 (2004), pp. 259–265. DOI: 10.1016/j.ultramic.2003.11.009.

[40] Roelie L. Kingma, Maria Fragiathaki, Harm J. Snijder, Bauke W. Dijkstra, Hubertus M. Verheij, Niek Dekker, and Maarten R. Egmond. "Unusual Catalytic Triad of *Escherichia coli* Outer Membrane Phospholipase A †." In: *Biochemistry* 39.33 (2000), pp. 10017–10022. DOI: 10.1021/bi000786d.

[41] Noriyuki Kodera, Mitsuru Sakashita, and Toshio Ando. "Dynamic proportional-integral-differential controller for high-speed atomic force microscopy." In: *Review of Scientific Instruments* 77.8 (2006). DOI: http://dx.doi.org/10.1063/1.2336113.

[42] Noriyuki Kodera, Hayato Yamashita, and Toshio Ando. "Active damping of the scanner for high-speed atomic force microscopy." In: *Review of Scientific Instruments* 76.5 (2005). DOI: http://dx.doi.org/10.1063/1.1903123.

[43] Noriyuki Kodera, Daisuke Yamamoto, Ryoki Ishikawa, and Toshio Ando. "Video imaging of walking myosin V by high-speed atomic force microscopy." In: *Nature* 468.7320 (2010), pp. 72–76. DOI: 10.1038/nature09450.

[44] J. Luirink, C. van der Sande, J. Tommassen, E. Veltkamp, F. K. De Graaf, and B. Oudega. "Effects of divalent cations and of phospholipase A activity on excretion of cloacin DF13 and lysis of host cells." In: *Journal of General Microbiology* 132.3 (1986), pp. 825–834. DOI: 10.1099/00221287-132-3-825.

[45] S. R. Manalis, S. C. Minne, and C. F. Quate. "Atomic force microscopy for high speed imaging using cantilevers with an integrated actuator and sensor." In: *Applied Physics Letters* 68.6 (1996), pp. 871–873. DOI: 10.1063/1.116528.

[46] T M McIntyre and R M Bell. "Escherichia coli mutants defective in membrane phospholipid synthesis: binding and metabolism of 1-oleoylglycerol 3-phosphate by a plsB deep rough mutant." In: *Journal of Bacteriology* 135.1 (1978), pp. 215–226.

[47] K B Merck, H de Cock, H M Verheij, and J Tommassen. "Topology of the outer membrane phospholipase A of Salmonella typhimurium." In: *Journal of Bacteriology* 179.11 (1997), pp. 3443–3450.

[48] Atsushi Miyagi and Simon Scheuring. "Automated force controller for amplitude modulation atomic force microscopy." In: *Review of Scientific Instruments* 87.5 (2016). DOI: http://dx.doi.org/10.1063/1.4950777.

[49] Atsushi Miyagi, Christophe Chipot, Martina Rangl, and Simon Scheuring. "High-speed atomic force microscopy shows that annexin V stabilizes membranes on the second timescale." In: *Nature Nanotechnology* (2016). DOI: 10.1038/nnano.2016.89.

[50] Doi Osamu, Ohki Misao, and Nojima Shoshichi. "Two kinds of phospholipase A and lysophospholipase in Escherichia coli." In: *Biochimica et Biophysica Acta (BBA) - Lipids and Lipid Metabolism* 260.2 (1972), pp. 244–258. DOI: 10.1016/0005-2760(72)90036-7.

[51] P. Patriarca, S. Beckerdite, and P. Elsbach. "Phospholipases and phospholipid turnover in Escherichia coli spheroplasts." In: *Biochimica et Biophysica Acta (BBA) - Lipids and Lipid Metabolism* 260.4 (1972), pp. 593–600. DOI: 10.1016/0005-2760(72)90008-2.

[52] V. Pedrotta and B. Witholt. "Isolation and characterization of the cis-trans-unsaturated fatty acid isomerase of Pseudomonas oleovorans GP012." In: *Journal of Bacteriology* 181.10 (1999), pp. 3256–3261.

[53] L. M. Picco, L. Bozec, A. Ulcinas, D. J. Engledew, M. Antognozzi, M. A. Horton, and M. J. Miles. "Breaking the speed limit with atomic force microscopy." In: *Nanotechnology* 18.4 (2007), p. 044030. DOI: 10.1088/0957-4484/18/4/044030.

[54] A. P. Pugsley and M. Schwartz. "Colicin E2 release: lysis, leakage or secretion? Possible role of a phospholipase." In: *The EMBO journal* 3.10 (1984), pp. 2393–2397.

[55] *RCSB PDB - Holdings Report*. http://www.rcsb.org/pdb/statistics/holdings.do. [Online; accessed 25-August-2016]. 2016.

[56] Tomas R. Rodriguez and Ricardo Garcia. "Theory of Q control in atomic force microscopy." In: *Applied Physics Letters* 82.26 (2003), pp. 4821–4823. DOI: 10.1063/1.1584790.

[57] Yusuke Sakiyama, Adam Mazur, Larisa E. Kapinos, and Roderick Y. H. Lim. "Spatiotemporal dynamics of the nuclear pore complex transport barrier resolved by high-speed atomic force microscopy." In: *Nature Nanotechnology* 11 (2016), pp. 719–723. DOI: 10.1038/nnano.2016.62.

[58] Carl J. Scandella and Arthur Kornberg. "Membrane-bound phospholipase A1 purified from Escherichia coli." In: *Biochemistry* 10.24 (1971), pp. 4447–4456.

[59] T. E. Schaeffer, J. P. Cleveland, F. Ohnesorge, D. A. Walters, and P. K. Hansma. "Studies of vibrating atomic force microscope cantilevers in liquid." In: *Journal of Applied Physics* 80.7 (1996), pp. 3622–3627. DOI: 10.1063/1.363308.

[60] G. Schitter and A. Stemmer. "Identification and open-loop tracking control of a piezoelectric tube scanner for high-speed scanning-probe microscopy." In: *IEEE Transactions on Control Systems Technology* 12.3 (2004), pp. 449–454. DOI: 10.1109/TCST.2004.824290.

[61] Thomas J. Silhavy, Daniel Kahne, and Suzanne Walker. "The Bacterial Cell Envelope." In: *Cold Spring Harbor Perspectives in Biology* 2.5 (2010). DOI: 10.1101/cshperspect.a000414.

[62] H. J. Snijder and B. W. Dijkstra. "Bacterial phospholipase A: structure and function of an integral membrane phospholipase." In: *Biochimica et Biophysica Acta (BBA)-Molecular and Cell Biology of Lipids* 1488.1 (2000), pp. 91–101.

[63] H. J. Snijder, I. Ubarretxena-Belandia, M. Blaauw, K. H. Kalk, H. M. Verheij, M. R. Egmond, N. Dekker, and B. W. Dijkstra. "Structural evidence for dimerization-regulated activation of an integral membrane phospholipase." In: *Nature* 401.6754 (1999), pp. 717–721. DOI: 10.1038/44890.

[64] T. Sulchek, S. C. Minne, J. D. Adams, D. A. Fletcher, A. Atalar, C. F. Quate, and D. M. Adderton. "Dual integrated actuators for extended range high speed atomic force microscopy." In: *Applied Physics Letters* 75.11 (1999), pp. 1637–1639. DOI: 10.1063/1.124779.

[65] T. Sulchek, G. G. Yaralioglu, C. F. Quate, and S. C. Minne. "Characterization and optimization of scan speed for tapping-mode atomic force microscopy." In: *Review of Scientific Instruments* 73.8 (2002), pp. 2928–2936. DOI: 10.1063/1.1488679.

[66] A. Taketo. "Sensitivity of Escherichia coli to viral nucleic acid. 8. Idiosyncrasy of Ca2+-dependent competence for DNA." In: *Journal of Biochemistry* 75.4 (1974), pp. 895–904.

[67] Iban Ubarretxena-Belandia, Leo Hozeman, Els van der Brink-van der Laan, Eward H. M. Pap, Maarten R. Egmond, Hubertus M. Verheij, and Niek Dekker. "Outer Membrane Phospholipase A Is Dimeric in Phospholipid Bilayers: A Cross-Linking and Fluorescence Resonance Energy Transfer Study †." In: *Biochemistry* 38.22 (1999), pp. 7398–7405. DOI: 10.1021/bi983077x.

[68] Takayuki Uchihashi, Noriyuki Kodera, and Toshio Ando. "Guide to video recording of structure dynamics and dynamic processes of proteins by high-speed atomic force microscopy." In: *Nature Protocols* 7.6 (2012), pp. 1193–1206. DOI: 10.1038/nprot.2012.047.

[69] M. B. Viani et al. "Fast imaging and fast force spectroscopy of single biopolymers with a new atomic force microscope designed for small cantilevers." In: *Review of Scientific Instruments* 70.11 (1999), pp. 4300–4303. DOI: 10.1063/1.1150069.

[70] M. B. Viani, L. I. Pietrasanta, J. B. Thompson, A. Chand, I. C. Gebeshuber, J. H. Kindt, M. Richter, H. G. Hansma, and P. K. Hansma. "Probing protein-protein interactions in real time." In: *Nature Structural Biology* 7.8 (2000), pp. 644–647. DOI: 10.1038/77936.

[71] D. A. Walters, J. P. Cleveland, N. H. Thomson, P. K. Hansma, M. A. Wendman, G. Gurley, and V. Elings. "Short cantilevers for atomic force microscopy." In: *Review of Scientific Instruments* 67.10 (1996), pp. 3583–3590. DOI: 10.1063/1.1147177.

[72] J. Weiss, S. Beckerdite-Quagliata, and P. Elsbach. "Determinants of the action of phospholipases A on the envelope phospholipids of Escherichia coli." In: *The Journal of Biological Chemistry* 254.21 (1979), pp. 11010–11014.

[73] G C Wright, J Weiss, K S Kim, H Verheij, and P Elsbach. "Bacterial phospholipid hydrolysis enhances the destruction of Escherichia coli ingested by rabbit neutrophils. Role of cellular and extracellular phospholipases." In: *Journal of Clinical Investigation* 85.6 (1990), pp. 1925–1935.

[74] Q. Zhong, D. Inniss, K. Kjoller, and V.B. Elings. "Fractured polymer/silica fiber surface studied by tapping mode atomic force microscopy." In: *Surface Science* 290.1 (1993), pp. L688 –L692. DOI: http://dx.doi.org/10.1016/0039-6028(93)90582-5.

[75] Qingze Zou, Kam K. Leang, Eman Sadoun, M. J. Reed, and Santosh Devasia. "Control issues in high-speed AFM for biological applications: Collagen imaging example." In: *Asian Journal of Control* 6.2 (2004), pp. 164–178.

APPENDIX

A.1 OPENING OF LIPOSOMES

When using Tris buffer without NaCl (20 mM Tris, 2 mM EDTA, pH 7.4), several issues concerning the sample preparation occurred: In case of the OmpLA sample reconstituted in POPC the membranes did not adsorb on the mica at all. In case of the OmpLA reconstituted in DLPC several patches were found, but they were unstable and frequently got lost during scanning. Another issue with that buffer was that the liposomes did not form single bilayers until a certain amount of Ca^{2+} or Mg^{2+} was added (see Figure 32). This is undesired, because the proteins could not be imaged under EDTA conditions. Therefore, NaCl was added to the buffer in most of the experiments to avoid these effects.

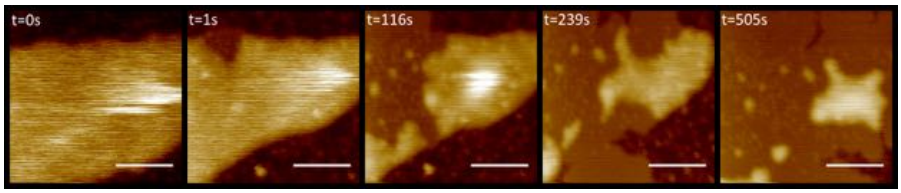

Figure 32: Opening of a DLPC proteoliposome. At t=1s the Ca^{2+} concentration was 1.3 mM. To receive single bilayers like in the last picture without Ca^{2+} or Mg^{2+} addition, in subsequent experiments 300 mM NaCl were added to the buffer. Scale bar: 100 nm. Full-color scale: 17 nm.

A.2 CHANGE IN APPEARANCE OF OMPLA IS REVERSIBLE

The change in appearance of the protein from vague protrusions to well defined structures upon the addition of Ca^{2+} or Mg^{2+} is reversible by the re-addition of EDTA (see Figure 33).

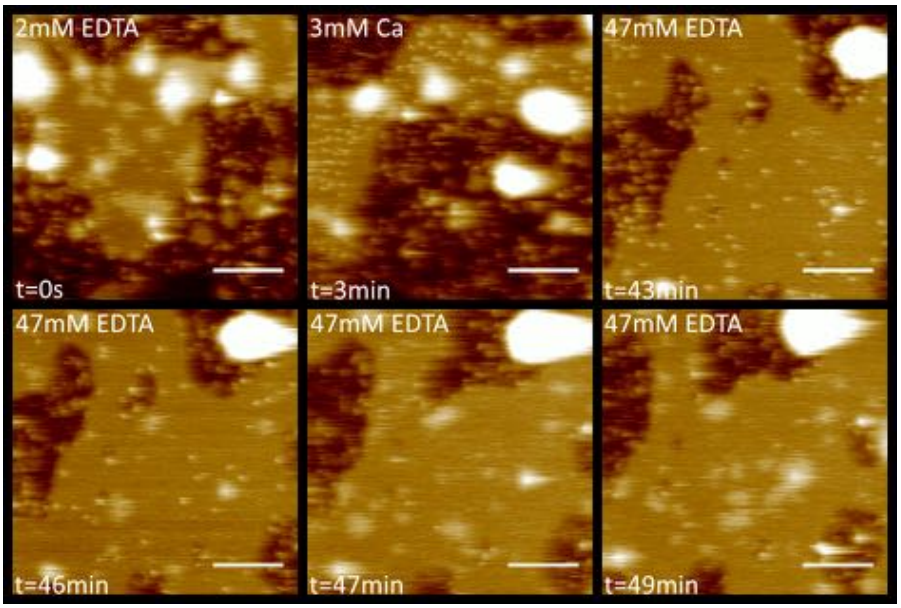

Figure 33: 3 mM Ca^{2+} were added into the buffer solution. As can be seen in the first and the second picture (same area slightly shifted to the right) within a few minutes the vague protrusions became well defined structures. When EDTA was added after 40 min, this effect was completely reversed within 10 min. Scale bar: 100 nm. Full-color scale: 10 nm.

UNIVERSITÄT BASEL

PHILOSOPHISCH-NATURWISSENSCHAFTLICHE FAKULTÄT

Erklärung zur wissenschaftlichen Redlichkeit

(beinhaltet Erklärung zu Plagiat und Betrug)

[redacted] / Masterarbeit *(nicht Zutreffendes bitte streichen)*

Titel der Arbeit *(Druckschrift)*:

High Speed Atomic Force Microscopy (HS-AFM): Direct Visualization of the Outer Membrane Phospholipase A (OmpLA) Activity

Name, Vorname *(Druckschrift)*: Rima, Luca

Matrikelnummer: 10-052-181

Hiermit erkläre ich, dass mir bei der Abfassung dieser Arbeit nur die darin angegebene Hilfe zuteil wurde und dass ich sie nur mit den in der Arbeit angegebenen Hilfsmitteln verfasst habe.

Ich habe sämtliche verwendeten Quellen erwähnt und gemäss anerkannten wissenschaftlichen Regeln zitiert.

Diese Erklärung wird ergänzt durch eine separat abgeschlossene Vereinbarung bezüglich der Veröffentlichung oder öffentlichen Zugänglichkeit dieser Arbeit.

■ ja ☐ nein

Ort, Datum: Marseille, 26.08.2016

Unterschrift: 

Dieses Blatt ist in die Bachelor-, resp. Masterarbeit einzufügen.

UNI BASEL